Chemi-ionization of mercury atoms: Potential curves and estimates of the total ionization cross sections

James S. Cohen,* Richard L. Martin, and Lee A. Collins

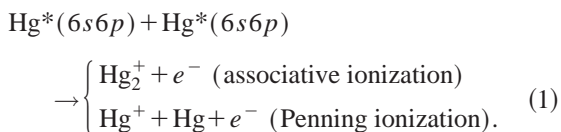*Theoretical Division, Los Alamos National Laboratory, Los Alamos, New Mexico 87545*

Potential curves for $Hg(6s6p) + Hg(6s6p)$ are calculated in the ΛS representation and transformed to the spin-orbit representation using empirical spin-orbit coupling constants. With these potential curves, total chemi-ionization cross sections are estimated using a black-sphere approximation for the short-range interaction. Long-range barriers, found in some of the potential curves, reduce the thermal-energy cross sections. Because these barrier heights are rather uncertain, the cross sections are also calculated with their suppression. The result, for $Hg(^3P_1) + Hg(^3P_0)$ collisions at 300 K, of 30–125 Å^2, overlaps the range of experimental measurements. For the only other pair considered in previous experiments, $Hg(^3P_0) + Hg(^3P_0)$, chemi-ionization was found to be energetically allowed but dynamically improbable. An upper limit, already lower than the posited measured value, was established, and the actual cross section is expected to be considerably smaller; this finding provides additional evidence that the reactants were misidentified in the experiment. The cross section for the statistically dominant metastable atoms $Hg(^3P_2) + Hg(^3P_2)$, 8–11 Å^2, is also relatively small. The chemi-ionization cross sections obtained for the other triplet reactants are 33–80 Å^2 for $Hg(^3P_1) + Hg(^3P_1)$, 17–31 Å^2 for $Hg(^3P_2) + Hg(^3P_0)$, and 15–22 Å^2 for $Hg(^3P_2) + Hg(^3P_1)$. The chemi-ionization cross sections for the singlet atom are large, 116–226 Å^2 for $Hg(^1P_1) + Hg(^3P_0)$, 161–285 Å^2 for $Hg(^1P_1) + Hg(^3P_1)$, 105–293 Å^2 for $Hg(^1P_1) + Hg(^3P_2)$, and 132–397 Å^2 for $Hg(^1P_1) + Hg(^1P_1)$. Though we do not yet have the autoionization widths required for quantitative distinction, the relative shapes of the neutral and ion potential curves suggest that most of the chemi-ionization will be of the associative, instead of the Penning type, even when the latter is energetically allowed.

I. INTRODUCTION

In chemi-ionization reactions, ionization occurs in thermal collisions of two atoms, using the electronic excitation energy to ionize the reactants [1]. Chemi-ionization is essentially a Franck-Condon process by which the relative kinetic energy and distance of the nuclei tend to be conserved in the transition. Depending on the relative values of the excitation energy and ionization potential, the result can be *Penning* or *associative* ionization. In *asymmetric* collisions, excitation of one atom may be sufficient to ionize the other, for example, the Penning ionization reaction $He^*(1s2s) + Hg \rightarrow He + Hg^+ + e^-$, where * designates the lowest manifold of excited states. In *symmetric* collisions, associative ionization may be possible if the interaction is strongly attractive, but generally a higher excitation is required or both atoms must be excited. For mercury, two ionization paths are possible,

$$Hg^*(6s6p) + Hg^*(6s6p)$$

$$\rightarrow \begin{cases} Hg_2^+ + e^- & \text{(associative ionization)} \\ Hg^+ + Hg + e^- & \text{(Penning ionization).} \end{cases} \quad (1)$$

The pairs $Hg(^3P_0) + Hg(^3P_0)$, $Hg(^3P_1) + Hg(^3P_0)$, $Hg(^3P_1) + Hg(^3P_1)$, $Hg(^3P_2) + Hg(^3P_0)$, and $Hg(^3P_2) + Hg(^3P_1)$ can only associatively ionize in thermal-energy collisions, while the pairs $Hg(^3P_2) + Hg(^3P_2)$, $Hg(^1P_1)$

$+ Hg(^3P_0)$, $Hg(^1P_1) + Hg(^3P_1)$, $Hg(^1P_1) + Hg(^3P_2)$, and $Hg(^1P_1) + Hg(^1P_1)$ can Penning or associatively ionize, as can be seen in Fig. 1.

Chemi-ionization is of particular importance in the modeling of fluorescent lamps [2–8], where it is an important loss mechanism. The reactions affect the ionization balance and excited-state distributions through subsequent recombination. It is of some importance whether the ionization is associative or Penning since dissociative recombination of the molecular ion is much more rapid than recombination with the atomic ion. Experimentally [9] the dissociative-recombination rate constant has been found to be ~ 200 times larger than the associative-ionization rate constant for $Hg(^3P_1) + Hg(^3P_0)$. Only the total ionization cross section (sum of the Penning and associative ionization cross sections) is calculated in the present work, although some qualitative observations about the anticipated relative contributions are made.

Three independent experiments [9–11] have measured associative ionization in mercury at thermal temperatures; they disagree with each other on the magnitude of the cross section by about a factor of three but, more importantly, disagree as to what states are involved, $Hg(^3P_0) + Hg(^3P_0)$ or $Hg(^3P_1) + Hg(^3P_0)$. In this regard, the dissociation energy D_0 of the product molecular ion Hg_2^+ is critical; it must be at least $I_P - 2E(^3P_0) = 1.10$ eV to enable associative ionization in collisions of $Hg(^3P_0) + Hg(^3P_0)$ at near-zero energy. Some studies (see Sec. II A) indicate a smaller value of D_0, while others indicate it is large enough, although this is not a sufficient condition to prove that associative ionization oc-
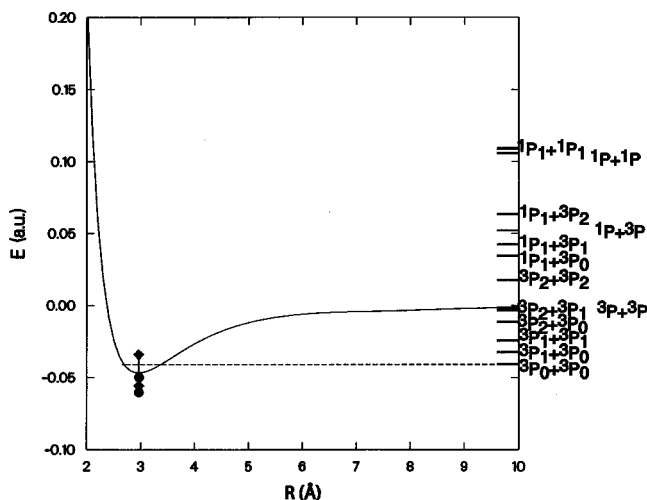
*Electronic address: cohen@lanl.gov

FIG. 1. Potential curve for Hg_2^+ and asymptotic energy levels (1 a.u. = 27.21 eV) for $Hg(6s6p) + Hg(6s6p)$ with and without spin-orbit coupling. The zero of the energy axis is taken as the energy of Hg (ground state) + Hg^+. The atomic ionization potential of Hg is 10.44 eV and the excitation energies of the two excited $(6s6p)$ atoms range from 9.33 to 13.41 eV relative to the ground-state atoms. The range of our theoretical dissociation energies is shown with circles, that of experimental dissociation energies with diamonds. The dashed line indicates the minimum dissociation energy required for associative ionization to occur in $Hg(^3P_0)$ + $Hg(^3P_0)$ collisions at zero incident energy.

curs in the actual dynamics. In the present work, we calculate the potential energy curves for Hg_2^+ as well as potential curves for Hg_2^* needed for all ten of the $Hg^*(6s6p)$ + $Hg^*(6s6p)$ reactions.

Besides the chemi-ionization reactions, energy pooling,

$$Hg^* + Hg^* \rightarrow Hg^{**} + Hg, \qquad (2)$$
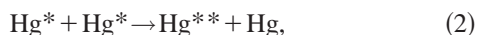
where Hg^{**} is an excitation to a shell $n \geq 7$, is possible. Reactions 1 and 2 compete, but chemi-ionization is expected to have the larger cross section when allowed; such a relationship has been observed experimentally [12,13]. Our potential curves are relevant to both, but the basis set is principally designed for chemi-ionization. In a discharge, the highly excited state Hg^{**} is fairly easily ionized by electron collisions so that the result may effectively be the same, albeit attained with an additional step.

II. POTENTIAL CURVES

A. Configuration-interaction calculations

Our theoretical approach [14] describes the interatomic interactions affecting chemi-ionization by a complex potential: the real part is the potential energy V and the imaginary part is (half) the autoionization width Γ. These quantities depend on the internuclear distance R and are different for each molecular state formed from the pair of reactant atomic states. We have calculated the potential curves with the *ab initio* code MESA [15]. It determines the molecular wave functions in the ΛS representation using a Gaussian orbital basis set and configuration interaction (CI) based on the self-

consistent-field (SCF) orbitals. Relativistic effects are important for atoms as heavy as mercury. The calculations utilize a "small-core" relativistic effective-core potential and associated double-zeta basis set due to Stevens *et al.* [16,17]. In this potential, the $5s$, $5p$, and $5d$ semicore orbitals are treated explicitly and not folded into the potential. At each internuclear distance R, the SCF molecular orbitals for the ground state of Hg_2 are determined. These SCF orbitals form the basis for a CI in which the 18 molecular orbitals originating from the semicore atomic orbitals are frozen, and a full four-electron CI is performed for the remaining electrons. This full valence CI generates correlated approximations to the ground and excited states.[1]

There have been a number of *ab initio* studies of the potential curves of $Hg^* + Hg$ [18–23],[2] but none of the curves arising from $Hg^* + Hg^*$, with both atoms asymptotically excited. The calculation is complicated by the fact that the $Hg(6s6p) + Hg(6s6p)$ states are partially embedded in an electronic continuum. It is not possible to include the infinite continuum of states, but the interactions are stabilized by doing a full CI. A further complication in the identification of curves comes from the configurations of $Hg^+ + Hg^-$.[3] These states start above the $^3P + {}^3P$ asymptote but plunge through the neutral manifold of states at finite values of R and, therefore, require careful disentanglement. This is a large calculation; with 45 virtual orbitals, as many as ~50 000 configurations result, depending on the symmetry. Up to 15 roots of these large matrices must be extracted; this is done using the Davidson method [25] and is the most computationally time-consuming part of the calculation. There are 36 distinct states in the ΛS representation having 18 different molecular symmetries $^{1,3,5}(\Sigma^{+,-}, \Pi, \Delta)_{g,u}$, where the numerical superscript gives the spin multiplicity, $+$ or $-$ the reflection symmetry of Σ states, Σ, Π, or Δ the component of electronic angular momentum along the internuclear axis (0, 1, or 2), and the subscript g or u, the parity. They are listed in Table I. The calculated ΛS potential energies are shown in Fig. 2 [26].

It can be seen that some of the otherwise attractive potential curves exhibit small barriers ($\lesssim 0.001$ a.u.) at large distances (6–8 Å). Such barriers could drastically reduce the ionization cross sections at low temperatures, but long-range barriers are notoriously difficult to get accurately in *ab initio* electronic-structure calculations. In addition to the attractive R^{-6} van der Waals potentials, some of the states are expected to have R^{-5} potentials, which may be attractive or repulsive. The latter interactions come from the long-range

---

[1] The four highest lying virtual orbitals were omitted from the CI, as they correspond primarily to the *s*-like components of *d* functions in the core and are not expected to contribute significantly to the valence correlation energy.

[2] Some of these results were actually based on calculations on the Mg_2 or Zn_2 molecules.

[3] The atomic negative ion Hg^- does not exist (i.e., the electron affinity is negative [24]), but such configurations are still important.

TABLE I. Symmetries of states formed from $Hg(6s6p) + Hg(6s6p)$ without spin-orbit coupling [Hund's case (a)]. The orbital angular momentum projections (m_{L_1}, m_{L_2}) on the internuclear axis are given after the molecular symmetry, and their designations in Tables III–XIII are given below.

$^3P + {}^3P$ singlet states

$^1\Sigma_g^+(00)$	$^1\Sigma_g^+(+-)$	$^1\Sigma_u^-(+-)$	$^1\Pi_g(+0)$	$^1\Pi_u(+0)$	$^1\Delta_g(++)$
E_1^g	E_2^g	E_1^u	E_3^g	E_2^u	E_4^g

$^3P + {}^3P$ triplet states

$^3\Sigma_u^+(00)$	$^3\Sigma_u^+(+-)$	$^3\Sigma_g^-(+-)$	$^3\Pi_g(+0)$	$^3\Pi_u(+0)$	$^3\Delta_u(++)$
E_3^u	E_4^u	E_5^g	E_6^g	E_5^u	E_6^u

$^3P + {}^3P$ quintet states

$^5\Sigma_g^+(00)$	$^5\Sigma_g^+(+-)$	$^5\Sigma_u^-(+-)$	$^5\Pi_g(+0)$	$^5\Pi_u(+0)$	$^5\Delta_g(++)$
E_7^g	E_8^g	E_7^u	E_9^g	E_8^u	E_{10}^g

$^1P + {}^3P$ triplet states

$^3\Sigma_g^+(-+)$	$^3\Sigma_g^-(+-)$	$^3\Sigma_u^+(-+)$	$^3\Sigma_u^-(+-)$	$^3\Sigma_g^+(00)$	$^3\Sigma_u^+(00)$
E_{11}^g	E_{12}^g	E_9^u	E_{10}^u	E_{13}^g	E_{11}^u
$^3\Pi_g(0+)$	$^3\Pi_g(+0)$	$^3\Pi_u(0+)$	$^3\Pi_u(+0)$	$^3\Delta_g(++)$	$^3\Delta_u(++)$
E_{14}^g	E_{15}^g	E_{12}^u	E_{13}^u	E_{16}^g	E_{14}^u

$^1P + {}^1P$ singlet states

$^1\Sigma_g^+(00)$	$^1\Sigma_g^+(+-)$	$^1\Sigma_u^-(+-)$	$^1\Pi_g(+0)$	$^1\Pi_u(+0)$	$^1\Delta_g(++)$
E_{17}^g	E_{18}^g	E_{15}^u	E_{19}^g	E_{16}^u	E_{20}^g

interaction of the quadrupole moments of the atoms, neither of which is in an S state [27]. Bumps appearing at smaller distances in the potential curves are generally due to avoided crossings.

In addition to the excited states, the potential curve of the molecular ion Hg_2^+ is also needed. This is a relatively simple calculation. Using the same core potential, basis set, and a full valence CI based on the Hg_2^+ SCF orbitals, we obtain a dissociation energy $D_e = 1.27$ eV at $R_e = 2.95$ Å, which may be compared with experimental values of 0.9 eV [28],
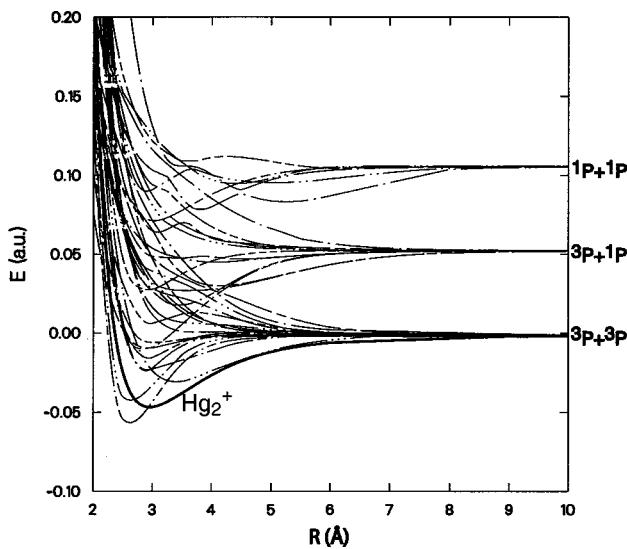
FIG. 2. *Ab initio* potential curves for $Hg(6s6p) + Hg(6s6p)$ and $Hg + Hg^+$ without spin-orbit coupling (in the ΛS representation) [26]. The molecular symmetry [in Hund's case (a)] is designated as follows: number dots=1+angular momentum of g states, number dashes=1+angular momentum of u states, except Σ_g^- =dot dash, and Σ_u^+=dash dot.

1.1 eV [29], and 1.40 ± 0.02 eV [30] and a previous theoretical value of 0.67 eV [31]. The largest of these values, from a photoionization experiment [30], is the most precise, but is possibly inconsistent with experiments [12,32], which observed excitation of Hg** above 9.0 eV. A dissociation energy of 1.4 eV would preclude dissociative-recombination excitation of Hg** above 9.0 eV [12], but emission from states lying above that level has been observed [12,32]. This interpretation supports a smaller value of $D_e \approx 1.0$ eV [33–35], but the observation may be alternatively explained by nonthermal electron collisions with Hg* or recombination with vibrationally excited Hg_2^+ [12].

We also did a hybrid (B3LYP) density-functional calculation [36,37] on Hg_2^+ and obtained $D_e = 1.50$ eV at $R_e = 3.02$ Å. Thus our two calculations bracket the precise experimental value, and both would allow associative ionization in thermal $Hg(^3P_0) + Hg(^3P_0)$ collisions. In subsequent considerations, we use the Hg_2^+ potential curve obtained in the configuration-interaction calculation since consistency with the excited-state calculations is most important.

B. Spin-orbit coupling

The above states are not yet usable to describe the observed interactions since spin-orbit coupling is essential to understanding the mercury atom or dimer. In the real atom, the ^3P and ^1P LS states are split into $^3P_0$, $^3P_1$, $^3P_2$, and $^1P_1$ levels. The spin-orbit matrix elements are derived from the experimental atomic energy levels. Because the molecule is symmetric and core breaking is weak, we assume that the same spin-orbit matrix elements can be used at finite internuclear distances; this approach proved satisfactory in earlier noble-gas excimer calculations [38].

The matrices representing the spin-orbit coupling are determined as symmetrized, spin-adapted sums over the ΛS

TABLE II. Symmetries of states formed from Hg(6s6p) +Hg(6s6p) with spin-orbit coupling [Hund's case (c)]. The number of times each molecular symmetry occurs is shown in parentheses if greater than one.

$^3P_2 + {}^3P_2$	$0_g^+(3), 0_u^-(2), 1_g(2), 1_u(2), 2_g(2), 2_u, 3_g, 3_u, 4_g$
$^3P_2 + {}^3P_1$	$0_g^+, 0_u^+, 0_g^-(2), 0_u^-(2), 1_g(3), 1_u(3), 2_g(2), 2_u(2), 3_g, 3_u$
$^3P_2 + {}^3P_0$	$0_g^+, 0_u^+, 1_g, 1_u, 2_g, 2_u$
$^3P_1 + {}^3P_1$	$0_g^+(2), 0_u^-, 1_g, 1_u, 2_g$
$^3P_1 + {}^3P_0$	$0_g^-(2), 0_u^-, 1_g, 1_u$
$^3P_0 + {}^3P_0$	0_g^+
$^1P_1 + {}^3P_2$	$0_g^+, 0_u^+, 0_g^-(2), 0_u^-(2), 1_g(3), 1_u(3), 2_g(2), 2_u(2), 3_g, 3_u$
$^1P_1 + {}^3P_1$	$0_g^+(2), 0_u^+(2), 0_g^-, 0_u^-, 1_g(2), 1_u(2), 2_g, 2_u$
$^1P_1 + {}^3P_0$	$0_g^-, 0_u^-, 1_g, 1_u$
$^1P_1 + {}^1P_1$	$0_g^+(2), 0_u^-, 1_g, 1_u, 2_g$

states. With spin-orbit coupling, the 36 ΛS [Hund's case (a)] states are turned into 90 spin-orbit states [Hund's case (c)], listed in Table II. For this purpose we need to transform the spin-orbit coupling matrix from the ΩS representation to the ΛS representation, in which the molecular potential curves are calculated. We start with the spin-orbit (SO) matrix for one excited $6s6p$ atom,

$$V_{SO}(LSj;L'S'j') = \begin{bmatrix} -\zeta & 0 & 0 & 0 \\ 0 & -\zeta/2 & 0 & \lambda\zeta/\sqrt{2} \\ 0 & 0 & \zeta/2 & 0 \\ 0 & \lambda\zeta/\sqrt{2} & 0 & \epsilon \end{bmatrix} \delta_{m_j,m_j'}, \quad (3)$$

where the order of the elements is $^3P_0$, $^3P_1$, $^3P_2$, and $^1P_1$, with parameters derived by Mies *et al.* [19], $\zeta = 4265.65$ cm^{-1}, $\lambda = 0.757693$, and $\epsilon = E(L=1,S=0) - E(L=1,S=1) = 11\,793.024$ cm^{-1}. This yields the experimental Hg($6s6p$, $^{2S+1}P_J$) energies correctly to three decimal places (in cm^{-1}).

For one atom,

$$|LSm_Lm_S\rangle = \sum_{j,m_j} \langle LSm_Lm_S|jm_j\rangle |jm_j\rangle. \quad (4)$$

The asymptotic limit of a molecule of spin S, without inversion or reflection symmetry, is given by

$$|R;L_1S_1L_2S_2m_{L_1}m_{L_2};\Lambda S\rangle$$

$$\sim \sum_{m_{S_1},m_{S_2}} \langle S_1m_{S_1}S_2m_{S_2}|Sm_S\rangle |L_1S_1m_{L_1}m_{S_1}\rangle$$

$$\times |L_2S_2m_{L_2}m_{S_2}\rangle, \quad (5)$$

where the asymptotes are designated by subscripts 1 and 2, $\Lambda = |m_{L_1} + m_{L_2}|$, and $m_S = m_{S_1} + m_{S_2}$. Note that there can be more than one molecular state with the same L,S asymptotes but distinguished by m_{L_1}, m_{L_2}.

We assume that the spins are not recoupled at finite R and that the asymptotic spin-orbit coupling constants are still a reasonable approximation at finite R. Spin-orbit interactions with other atomic configurations [39], e.g., $6s7p$ or those that would open the core, are partially taken into account by the effective values of the parameters. We neglect spin-other orbit and spin-spin couplings as well as two-center effects and the small hyperfine interaction with the nuclear spins.

With these assumptions,

$$|R;L_1S_1L_2S_2m_{L_1}m_{L_2};\Lambda S\rangle$$

$$\approx \sum_{j_1,m_{j_1},j_2,m_{j_2}} \langle L_1S_1m_{L_1}m_{S_1}|j_1m_{j_1}\rangle\langle L_2S_2m_{L_2}m_{S_2}|j_2m_{j_2}\rangle$$

$$\times \langle S_1m_{S_1}S_2m_{S_2}|Sm_S\rangle |R;S_1j_1S_2j_2;\Omega m_{j_1}m_{j_2}\rangle, \quad (6)$$

TABLE III. Spin-orbit matrix for 0_g^+ states. $a \equiv 2^{-1/2}$, $b \equiv 3^{-1/2}$.

E_1^g	0	0	$a^{-1}b\zeta$	0	0	0	0	0	$-b\lambda\zeta$	0	0	0
0	E_2^g	$a^{-1}b\zeta$	$-b\zeta$	0	0	0	0	$ab\lambda\zeta$	0	$-ab\lambda\zeta$	0	0
0	$a^{-1}b\zeta$	E_5^g	$a^3\zeta$	0	$b\zeta$	$-a^3\zeta$	0	0	0	$a^2\lambda\zeta$	0	0
$a^{-1}b\zeta$	$-b\zeta$	$a^3\zeta$	$E_6^g - a^4\zeta$	$-a^2b\zeta$	$a^3b\zeta$	$a^4\zeta$	$-a^2\zeta$	$a^3\lambda\zeta$	$a^3\lambda\zeta$	0	0	0
0	0	0	$-a^2b\zeta$	E_7^g	0	$a^2b^{-1}\zeta$	0	0	$-ab\lambda\zeta$	0	0	0
0	0	$b\zeta$	$a^3b\zeta$	0	E_8^g	$a^3b^{-1}\zeta$	0	$-b\lambda\zeta$	0	$-a^2b\lambda\zeta$	0	0
0	0	$-a^3\zeta$	$a^4\zeta$	$a^2b^{-1}\zeta$	$a^3b^{-1}\zeta$	$E_9^g - a^4\zeta$	$a^2\zeta$	$a^3\lambda\zeta$	$a^3\lambda\zeta$	0	0	0
0	0	0	$-a^2\zeta$	0	0	$a^2\zeta$	$E_{10}^g - \zeta$	0	0	$a\lambda\zeta$	0	0
0	$ab\lambda\zeta$	0	$a^3\lambda\zeta$	0	$-b\lambda\zeta$	$a^3\lambda\zeta$	0	E_{12}^g	$-a^2\zeta$	0	0	$a\lambda\zeta$
$-b\lambda\zeta$	0	0	$a^3\lambda\zeta$	$-ab\lambda\zeta$	0	$a^3\lambda\zeta$	0	$-a^2\zeta$	E_{14}^g	0	0	$a\lambda\zeta$
0	$-ab\lambda\zeta$	$a^2\lambda\zeta$	0	0	$-a^2b\lambda\zeta$	0	$a\lambda\zeta$	0	0	$E_{15}^g - a^2\zeta$	$\lambda\zeta$	0
0	0	0	0	0	0	0	0	0	0	$\lambda\zeta$	E_{17}^g	0
0	0	0	0	0	0	0	0	$a\lambda\zeta$	$a\lambda\zeta$	0	0	E_{18}^g

where $\Omega = |m_{j_1} + m_{j_2}|$, $m_{j_1} = m_{L_1} + m_{S_1}$, and $m_{j_2} = m_{L_2} + m_{S_2}$. The quantum numbers m_{j_1}, m_{j_2} distinguish different molecular states having the same Ω and asymptotic S_1, j_1, S_2, j_2. The symmetrized molecular wave function is then given by

$$|R; L_1 S_1 L_2 S_2 m_{L_1} m_{L_2}; \Lambda S p r\rangle \approx [c_r(1)^2 + c_r(2)^2]^{-1/2} [c_p(1)^2 + c_p(2)^2]^{-1/2} \sum_{i=1}^{2} c_r(i) \sum_{k=1}^{2} c_p(k)$$

$$\times \sum_{j_1, m_{j_1}, j_2, m_{j_2}} \langle L_1 S_1 m_{L_1} m_{S_1} | j_1 m_{j_1} \rangle \langle L_2 S_2 m_{L_2} m_{S_2} | j_2 m_{j_2} \rangle \langle S_1 m_{S_1} S_2 m_{S_2} | S m_S \rangle$$

$$\times |R; S_1 j_1 S_2 j_2; \Omega m_{j_1} m_{j_2} \rangle, \tag{7}$$

where p designates the parity (inversion symmetry) of the homonuclear molecule and r designates the reflection symmetry of $\Omega = 0$ states. The symmetrization coefficients are given by

$$c_r(1) = 1,$$

$$c_r(2) = \begin{cases} (-1)^S r & \text{if } \Omega = 0 \text{ and } \{\Lambda \neq 0 \text{ or } [(S_1, L_1) \neq (S_2, L_2) \text{ and } m_{L_1} \neq 0]\} \\ 0 & \text{otherwise}, \end{cases} \tag{8}$$

with $r = +1(-1)$ for $0^+(0^-)$ states and

$$c_p(1) = 1,$$

$$c_p(2) = \begin{cases} (-1)^{(S_1 + S_2 + S)} p & \text{if } (S_1, L_1, M_{L_1}) \neq (S_2, L_2, M_{L_2}) \\ 0 & \text{otherwise}, \end{cases} \tag{9}$$

with $p = +1(-1)$ for $g(u)$ states.

We designate the initial and final states by unprimed and primed quantum numbers, respectively, and transform the spin-orbit coupling matrix to the ΛS representation, where the *ab initio* potential curves V_0 are calculated. The final form is given by

$$V^{(\Omega r p)}(R L_1 S_1 L_2 S_2 m_{L_1} m_{L_2} \Lambda S p r_0; R L_1' S_1' L_2' S_2' m_{L_1}' m_{L_2}' \Lambda' S' p r_0')$$

$$= \langle R L_1 S_1 L_2 S_2 m_{L_1} m_{L_2} \Lambda S p r_0 | H_e^{(LS)} + V_{SO} | R L_1' S_1' L_2' S_2' m_{L_1}' m_{L_2}' \Lambda' S' p r_0' \rangle$$

$$= V_0(R L_1 S_1 L_2 S_2 m_{L_1} m_{L_2} \Lambda S p r_0) \delta_{L_1, L_1'} \delta_{L_2, L_2'} \delta_{S_1, S_1'} \delta_{S_2, S_2'} \delta_{S, S'} \delta_{m_{L_1}, m_{L_1}'} \delta_{m_{L_2}, m_{L_2}'} \delta_{\Lambda, \Lambda'}$$

$$+ [c_r(1)^2 + c_r(2)^2]^{-1/2} [c_p(1)^2 + c_p(2)^2]^{-1/2} [c_r'(1)^2 + c_r'(2)^2]^{-1/2} [c_p'(1)^2 + c_p'(2)^2]^{-1/2}$$

$$\times \sum_{i=1}^{2} c_r(i) \sum_{k=1}^{2} c_p(k) \sum_{i'=1}^{2} c_r'(i') \sum_{k'=1}^{2} c_p'(k') \sum_{\substack{j_1, j_2, j_1', j_2' \\ m_{j_1}, m_{j_2}, m_{j_1}', m_{j_2}'}} [V_{SO}(L_1 S_1 j_1; L_1' S_1' j_1') \delta_{L_2, L_2'} \delta_{S_2, S_2'}$$

$$+ V_{SO}(L_2 S_2 j_2; L_2' S_2' j_2') \delta_{L_1, L_1'} \delta_{S_1, S_1'}] \langle L_1 S_1 m_{L_1} m_{S_1} | j_1 m_{j_1} \rangle \langle L_2 S_2 m_{L_2} m_{S_2} | j_2 m_{j_2} \rangle$$

$$\times \langle L_1' S_1' m_{L_1}' m_{S_1}' | j_1' m_{j_1}' \rangle \langle L_2' S_2' m_{L_2}' m_{S_2}' | j_2' m_{j_2}' \rangle \langle S_1 m_{S_1} S_2 m_{S_2} | S m_S \rangle \langle S_1' m_{S_1}' S_2' m_{S_2}' | S' m_S' \rangle \, \delta_{m_{j_1}, m_{j_1}'} \delta_{m_{j_2}, m_{j_2}'}, \tag{10}$$

where r_0 designates the reflection symmetry of the $\Lambda = 0$ states. All nonzero values of Ω satisfying the triangle inequalities $|\Omega \pm \Lambda| \leq S$ occur. $\Omega = 0$ states occur for $|\Omega - \Lambda| \leq S$ if $S + r_0 + r$ is even and for $|\Omega + \Lambda| \leq S$ if $S + r_0 + r$ is odd. By virtue of the δ functions and Clebsch-Gordan coefficients, $m_{j_1} = m_{j_1}'$, $m_{j_2} = m_{j_2}'$, and $m_{j_1} + m_{j_2} = m_{j_1}' + m_{j_2}' = \Omega$, so three of the sums in Eq. (10) are trivial. It can be seen that the non-Σ states contribute in pairs to both the 0^+ and 0^- states. The $\Sigma^\pm$ states contribute to only one of the

0^+ or 0^-, the same reflection symmetry for even S and the opposite for odd S. The parity p is not affected by spin-orbit coupling. In all cases presently considered, $L_1 = L_2 = 1$.

The analytic matrices resulting from Eq. (10) are given in Tables III–XIII for the 0_g^+, 0_g^-, 1_g, 2_g, 3_g, 4_g, 0_u^+, 0_u^-, 1_u, 2_u, and 3_u states, respectively. The 4_u sum vanishes, and, as can be seen in Table VIII, the 4_g state is pure $^5\Delta_g$, shifted by energy ζ. The unitary transformations yield symmetric matrices, but they are shown in full for clarity. These

TABLE IV. Spin-orbit matrix for 0_g^- states. $a \equiv 2^{-1/2}$.

$E_6^g - a^4\zeta$	$a^4\zeta$	$-a^2\zeta$	$a^3\lambda\zeta$	$-a^2\lambda\zeta$	$a^3\lambda\zeta$	0
$a^4\zeta$	$E_9^g - a^4\zeta$	$a^2\zeta$	$a^3\lambda\zeta$	$a^2\lambda\zeta$	$a^3\lambda\zeta$	0
$-a^2\zeta$	$a^2\zeta$	$E_{10}^g - \zeta$	0	0	0	$a\lambda\zeta$
$a^3\lambda\zeta$	$a^3\lambda\zeta$	0	E_{11}^g	0	$a^2\zeta$	0
$-a^2\lambda\zeta$	$a^2\lambda\zeta$	0	0	E_{13}^g	0	$a\zeta$
$a^3\lambda\zeta$	$a^3\lambda\zeta$	0	$a^2\zeta$	0	E_{14}^g	0
0	0	$a\lambda\zeta$	0	$a\zeta$	0	$E_{15}^g - a^2\zeta$

matrices take all molecular symmetries into account and are irreducible. In particular, the $\Omega=0$ states, in Tables III, IV, IX, and X, separate 0^+ and 0^- states, which has not always been done [38,19]. These matrix elements depend only on the *ab initio* Hund's case (a) energies, as a function of R, and the two fixed spin-orbit parameters ζ and λ. Before the numerical diagonalization, the *ab initio* asymptotic energies are shifted slightly to agree with the experimental values. In all cases, the energies obtained in the $R\rightarrow\infty$ limit then agree precisely with the experimental atomic energies.

The matrices $V^{(\Omega rp)}$ are diagonalized to get the potential curves with spin-orbit coupling as a function of R as linear combinations of the $m_{L_1} m_{L_2} \Lambda S$ states. In the adiabatic description of chemi-ionization, these states are uncoupled, but, more precisely, transitions may sometimes occur between them due to dynamical effects. A case where such coupling is essential is found in the $\mathrm{Hg}(^3P_0) + \mathrm{Hg}(^3P_0)$ reaction.

III. CHEMI-IONIZATION CONSIDERATIONS

A. Model

The chemi-ionization reactions are described by complex potentials of the form [14]

$$W(R) = V(R) - \frac{i}{2}\Gamma(R). \tag{11}$$

The interatomic potentials, for the resonant states ϕ_r partially embedded in the electronic continuum, are

$$V(R) = \langle \phi_r | H | \phi_r \rangle, \tag{12}$$

where H is the total Hamiltonian. The *ab initio* calculations are performed in the ΛS representation and spin-orbit coupling is taken into account as described in Sec. II B.

The autoionization width is given by the on-shell expression

$$\Gamma = 2\pi\rho_E |\langle \mathcal{A}\phi_+ \chi_e(E) | H - E | \phi_r \rangle|^2, \tag{13}$$

where ϕ_+ is the molecular-ion wave function, $\chi_e(E)$ is the scattering wave function of the emitted electron at energy E, $\mathcal{A}$ is the antisymmetrizing operator, and ρ_E is the corresponding density of states. We have not calculated the ionization widths directly but can make preliminary estimates of the chemi-ionization cross sections by taking into account the following expected behaviors:

TABLE V. Spin-orbit matrix for 1_g states. $a \equiv 2^{-1/2}$, $b = 3^{-1/2}$.

E_3^g	$ab\zeta$	$ab\zeta$	0	0	0	0	0	$a^2b\lambda\zeta$	$a^2b\lambda\zeta$	$-a^2b\lambda\zeta$	0	$-a^2b\lambda\zeta$	0
$ab\zeta$	E_5^g	$a^4\zeta$	$a^4\zeta$	$a^4\zeta$	$a^2\zeta$	0	$-a^3\zeta$	0	$-a^3\lambda\zeta$	$-a^3\lambda\zeta$	0	$a^3\lambda\zeta$	0
$ab\zeta$	$a^4\zeta$	E_6^g	$a^4\zeta$	$a^2\zeta$	$a^2\zeta$	$-a^3\zeta$	0	0	$a^3\lambda\zeta$	$a^3\lambda\zeta$	0	$a^3\lambda\zeta$	0
0	$a^4\zeta$	$a^4\zeta$	E_7^g	$a^3b^{-1}\zeta$	$a^3\zeta$	$a^2\zeta$	0	0	$a^3\lambda\zeta$	$a^3\lambda\zeta$	0	$a^3\lambda\zeta$	0
0	$a^4\zeta$	$a^2\zeta$	$a^3b^{-1}\zeta$	E_8^g	$a^4b^{-1}\zeta$	$a^3\zeta$	$a^3\zeta$	0	$a^3\lambda\zeta$	$-a^3\lambda\zeta$	0	$-a^3\lambda\zeta$	0
0	$a^2\zeta$	$a^2\zeta$	$a^3\zeta$	$a^4b^{-1}\zeta$	E_9^g	$a^3b^{-1}\zeta$	0	0	$ab\lambda\zeta$	$ab\lambda\zeta$	0	$ab\lambda\zeta$	0
0	0	$-a^3\zeta$	$a^2\zeta$	$a^3\zeta$	$a^3b^{-1}\zeta$	$E_{10}^g - a^2\zeta$	0	0	$a^2\lambda\zeta$	$a^2\lambda\zeta$	0	$-a^2\lambda\zeta$	0
0	$-a^3\zeta$	0	0	$a^3\zeta$	0	0	$E_{11}^g - a^2\zeta$	0	$-a^2\lambda\zeta$	$-a^2\lambda\zeta$	0	$-a^2\lambda\zeta$	$-a^2\lambda\zeta$
$a^2b\lambda\zeta$	0	0	0	0	0	0	0	$E_{12}^g + a^2\zeta$	0	0	0	0	0
$a^2b\lambda\zeta$	$-a^3\lambda\zeta$	$a^3\lambda\zeta$	$a^3\lambda\zeta$	$a^3\lambda\zeta$	$ab\lambda\zeta$	$a^2\lambda\zeta$	$-a^2\lambda\zeta$	0	E_{13}^g	$a^2\zeta$	$a^2\zeta$	0	$-a^2\lambda\zeta$
$-a^2b\lambda\zeta$	$-a^3\lambda\zeta$	$a^3\lambda\zeta$	$a^3\lambda\zeta$	$-a^3\lambda\zeta$	$ab\lambda\zeta$	$a^2\lambda\zeta$	$-a^2\lambda\zeta$	0	$a^2\zeta$	E_{14}^g	$a^2\zeta$	0	0
0	0	0	0	0	0	0	0	0	$a^2\zeta$	$a^2\zeta$	E_{15}^g	0	$a^2\lambda\zeta$
$-a^2b\lambda\zeta$	$a^3\lambda\zeta$	$a^3\lambda\zeta$	$a^3\lambda\zeta$	$-a^3\lambda\zeta$	$ab\lambda\zeta$	$-a^2\lambda\zeta$	$-a^2\lambda\zeta$	0	0	0	0	$E_{16}^g - a^2\zeta$	$a^2\lambda\zeta$
0	0	0	0	0	0	0	$-a^2\lambda\zeta$	0	$-a^2\lambda\zeta$	0	$a^2\lambda\zeta$	$a^2\lambda\zeta$	E_{19}^g

TABLE VI. Spin-orbit matrix for 2_g states. $a \equiv 2^{-1/2}$, $b \equiv 3^{-1/2}$.

E_4^g	$b\zeta$	0	0	0	0	0	$ab\lambda\zeta$	$-ab\lambda\zeta$	0
$b\zeta$	$E_6^g + a^4\zeta$	$-a^2\zeta$	$a^3\zeta$	$a^4\zeta$	$-a^3 b\zeta$	$-a^3\lambda\zeta$	0	$a^3\lambda\zeta$	0
0	$-a^2\zeta$	E_7^g	0	$a^2\zeta$	0	$-a\lambda\zeta$	0	0	0
0	$a^3\zeta$	0	E_8^g	$a^3\zeta$	0	0	$-a^2\lambda\zeta$	0	0
0	$a^4\zeta$	$a^2\zeta$	$a^3\zeta$	$E_9^g + a^4\zeta$	$a^3 b^{-1}\zeta$	$a^3\lambda\zeta$	0	$-a^3\lambda\zeta$	0
0	$-a^3 b\zeta$	0	0	$a^3 b^{-1}\zeta$	E_{10}^g	0	$a^2 b\lambda\zeta$	$b\lambda\zeta$	0
0	$-a^3\lambda\zeta$	$-a\lambda\zeta$	0	$a^3\lambda\zeta$	0	E_{14}^g	0	$a^2\zeta$	$-a\lambda\zeta$
$ab\lambda\zeta$	0	0	$-a^2\lambda\zeta$	0	$a^2 b\lambda\zeta$	0	$E_{15}^g + a^2\zeta$	0	0
$-ab\lambda\zeta$	$a^3\lambda\zeta$	0	0	$-a^3\lambda\zeta$	$b\lambda\zeta$	$a^2\zeta$	0	E_{16}^g	$a\lambda\zeta$
0	0	0	0	0	0	$-a\lambda\zeta$	0	$a\lambda\zeta$	E_{20}^g

(1) The potential curves arising from the asymptote of the reactant pair of atoms are most important for chemi-ionization, though other curves may participate via curve crossings.

(2) The attractive curves contribute most to thermal chemi-ionization since the ionization width can be expected to decrease exponentially with increasing internuclear distance.

(3) The ion core plus free electron can be in a singlet or triplet state, and its interaction with the resonant state conserves spin. Thus quintet ΛS states cannot chemi-ionize, and spin-orbit states that have mainly quintet parentage will have widths correspondingly reduced.

(4) The ionization widths tend to be larger when the energies of the ejected electrons are small and to be approximately proportional to the overlap of the two atomic charge densities.

The approach we use to estimate the cross sections is a black-sphere model in which ionization is assumed to occur if and only if the classical turning point is less than $R_0 = \min(R_x, R_s)$, where R_x is the distance at which the neutral potential energy becomes higher than that of the molecular ion [infinity for $Hg(^3P_2) + Hg(^3P_2)$ and higher asymptotes] and R_s is the black-sphere radius. We take, as a compromise, $R_s = 4$ Å in all cases—by point (4) above, chemi-ionization in the lower-lying states might be favored by being closer to the ion curve, but the higher states might be favored by their smaller atomic ionization potentials and correspondingly greater overlaps. For the lowest four asymptotes ($^3P_0 + {}^3P_0$, $^3P_1 + {}^3P_0$, $^3P_1 + {}^3P_1$, and $^3P_2 + {}^3P_0$), $R_x \lesssim R_s$ and the results are fairly insensitive to the choice of R_s, but for the higher asymptotes R_s is essential.

Ignoring, for the moment, the three-turning-point cases, which may arise from long-range barriers or curve crossings, the largest impact parameter b_0 that will penetrate to $R = R_0$ in a collision at energy E satisfies

$$V(R_0) + \frac{E b_0^2}{R_0^2} = E, \tag{14}$$

so

$$b_0 = \left(1 - \frac{V(R_0)}{E}\right)^{1/2} R_0 \tag{15}$$

and the cross section is

$$\sigma(E) = \pi b_0^2 = \pi R_0^2 \left(1 - \frac{V(R_0)}{E}\right). \tag{16}$$

Since the largest contributions to thermal reactions are due to attractive potential curves, which can bring in large impact parameters, the cross sections can be much larger than πR_0^2 at low collision energies—up to one order of magnitude at 300 K. A cross section of the form of Eq. (16) has the peculiar property that the thermal average cross section, integrated over a Maxwellian distribution, is of the same form,

$$\bar{\sigma}(T) = \pi R_0^2 \left(1 - \frac{V(R_0)}{kT}\right). \tag{17}$$

If, at some distance $R > R_0$,

$$V(R) + \frac{E b_0^2}{R^2} > E, \tag{18}$$

then the cross section will be reduced. For convenience, we define

$$b_x = \left(1 - \frac{V(R_x)}{E}\right)^{1/2} R_x, \tag{19}$$

$$b_s = \left(1 - \frac{V(R_s)}{E}\right)^{1/2} R_s, \tag{20}$$

and

TABLE VII. Spin-orbit matrix for 3_g states. $a \equiv 2^{-1/2}$.

$E_9^g + a^2\zeta$	$a^2\zeta$	$-a^2\lambda\zeta$
$a^2\zeta$	$E_{10}^g + a^2\zeta$	$a^2\lambda\zeta$
$-a^2\lambda\zeta$	$a^2\lambda\zeta$	$E_{16}^g + a^2\zeta$

TABLE VIII. Spin-orbit matrix for 4_g states.

$E_{10}^g + \zeta$

TABLE IX. Spin-orbit matrix for 0_u^+ states. $a \equiv 2^{-1/2}$.

$E_5^u - a^4\zeta$	$a^4\zeta$	$a^3\lambda\zeta$	$-a^3\lambda\zeta$	0
$a^4\zeta$	$E_8^u - a^4\zeta$	$a^3\lambda\zeta$	$-a^3\lambda\zeta$	0
$a^3\lambda\zeta$	$a^3\lambda\zeta$	E_{10}^u	$-a^2\zeta$	0
$-a^3\lambda\zeta$	$-a^3\lambda\zeta$	$-a^2\zeta$	E_{12}^u	0
0	0	0	0	$E_{13}^u - a^2\zeta$

$$b_b = \min\left[\left(1 - \frac{V(R)}{E}\right)^{1/2} R\right]$$

$$\text{for} \quad R \geqslant \min(R_x, R_s) \quad \text{and} \quad V(R) \leqslant E. \quad (21)$$

We define R_b to be the value of R that maximizes $V(R) + Eb_b^2/R^2$ at $R \geqslant \min(R_x, R_s)$. Then the cross section without a barrier is

$$\sigma^{(nb)}(E) = \pi[\min(b_x, b_s)]^2, \quad (22)$$

and with a barrier,

$$\sigma^{(b)}(E) = \pi[\min(b_x, b_s, b_b)]^2. \quad (23)$$

Associative and Penning ionization cannot be quantitatively separated, or electron energy distributions obtained, by the present model. The total chemi-ionization cross sections are given by a statistically (angular momentum) weighted sum over all the potential curves arising from the pair of reactants $i \equiv {}^{2S+1}P_J$ and $i' \equiv {}^{2S'+1}P_{J'}$,

$$\sigma_{i+i'} = (2j_i + 1)^{-1}(2j_{i'} + 1)^{-1}(2 - \delta_{i,i'})^{-1}$$

$$\times \sum_{\Omega, r} (2 - \delta_{\Omega,0})\sigma_{i+i'}^{(\Omega r)}, \quad (24)$$

where the sum goes over the molecular states listed in Table II. This sum reflects the double degeneracy of the $\Omega \neq 0$ states and the pairing of g-u states in the case of nonidentical states.

In the general case, including Eq. (23), the thermal average of the cross section is not as simple as Eq. (17) and is obtained by 15-point Gauss-Laguerre quadrature of the integral,

$$\bar{\sigma}_{i+i'}(T) = (kT)^{-2} \int_0^\infty \sigma_{i+i'}(E)E \exp(-E/kT)dE, \quad (25)$$

at temperature T.

B. Cross sections

The chemi-ionization cross sections are calculated in the black-sphere approximation. Because of the uncertainty in the long-range parts of the potential curves and the sensitivity of the thermal reaction to this region, we present cross sections both with and without the potential barriers. Tunneling can be expected to be quite improbable for the heavy mercury atoms, so the chemi-ionization reaction will almost certainly not occur at collision energies much below the barrier height (making the Maxwellian tail particularly important). Certainly the centrifugal effect is real; however, the effective barriers depend on the sum of the centrifugal potential and the various long-range interatomic forces. The barriers seen in the *ab initio* curves generally appear in the region $R = 6$–8 Å. Forces, repulsive or attractive, at smaller distances are largely due to the molecular electron density. Based on these considerations, the test calculations suppressing long-range effects were done by ignoring barriers occurring at $R > 5$ Å, but not modifying the potentials at $R < 5$ Å.

We now consider each of the ten possible reactions separately at specific energy $E = kT = 0.000\,95$ a.u. and the thermal average at $T = 300$ K. The relevant parameters for the various potential curves contributing to the cross sections at this energy are given in Table XIV.

1. $Hg(^3P_0) + Hg(^3P_0)$

The potential curves relevant to associative ionization in collisions of two $Hg(^3P_0)$ atoms are shown in Fig. 3. From this asymptote there is only one potential curve (of 0_g^+ symmetry), and it does not cross the molecular-ion curve. Thus ionization is *adiabatically* forbidden. However, this potential curve has an avoided crossing with a potential curve, arising from the ${}^3P_1 + {}^3P_1$ asymptote, which does cross the molecular ion. At the avoided crossing, there is a finite probability P_{hop} of switching curves, which can be estimated by the

TABLE X. Spin-orbit matrix for 0_u^- states. $a \equiv 2^{-1/2}$, $b \equiv 3^{-1/2}$.

E_1^u	0	$a^{-1}b\zeta$	$-b\zeta$	0	0	$ab\lambda\zeta$	0	0	$-ab\lambda\zeta$	0
0	E_3^u	0	$a^2\zeta$	0	$a^2\zeta$	0	0	$a\lambda\zeta$	0	0
$a^{-1}b\zeta$	0	E_4^u	$a^3\zeta$	$b\zeta$	$-a^3\zeta$	0	0	0	$a^2\lambda\zeta$	0
$-b\zeta$	$a^2\zeta$	$a^3\zeta$	$E_5^u - a^4\zeta$	$a^3b\zeta$	$a^4\zeta$	$a^3\lambda\zeta$	$a^2\lambda\zeta$	$-a^3\lambda\zeta$	0	0
0	0	$b\zeta$	$a^3b\zeta$	E_7^u	$a^3b^{-1}\zeta$	$-b\lambda\zeta$	0	0	$-a^2b\lambda\zeta$	0
0	$a^2\zeta$	$-a^3\zeta$	$a^4\zeta$	$a^3b^{-1}\zeta$	$E_8^u - a^4\zeta$	$a^3\lambda\zeta$	$-a^2\lambda\zeta$	$-a^3\lambda\zeta$	0	0
$ab\lambda\zeta$	0	0	$a^3\lambda\zeta$	$-b\lambda\zeta$	$a^3\lambda\zeta$	E_9^u	0	$a^2\zeta$	0	$a\lambda\zeta$
0	0	0	$a^2\lambda\zeta$	0	$-a^2\lambda\zeta$	0	E_{11}^u	0	$a\zeta$	0
0	$a\lambda\zeta$	0	$-a^3\lambda\zeta$	0	$-a^3\lambda\zeta$	$a^2\zeta$	0	E_{12}^u	0	$-a\lambda\zeta$
$-ab\lambda\zeta$	0	$a^2\lambda\zeta$	0	$-a^2b\lambda\zeta$	0	0	$a\zeta$	0	$E_{13}^u - a^2\zeta$	0
0	0	0	0	0	0	$a\lambda\zeta$	0	$-a\lambda\zeta$	0	E_{15}^u

TABLE XII. Spin-orbit matrix for 2_u states. $a \equiv 2^{-1/2}$.

$E_5^u + a^4\zeta$	$a^3\zeta$	$a^3\zeta$	$a^4\zeta$	$a^3\lambda\zeta$	0	$a^3\lambda\zeta$
$a^3\zeta$	E_6^u	0	$a^3\zeta$	0	$a^2\lambda\zeta$	0
$a^3\zeta$	0	E_7^u	$a^3\zeta$	0	$-a^2\lambda\zeta$	0
$a^4\zeta$	$a^3\zeta$	$a^3\zeta$	$E_8^u + a^4\zeta$	$-a^3\lambda\zeta$	0	$-a^3\lambda\zeta$
$a^3\lambda\zeta$	0	0	$-a^3\lambda\zeta$	E_{12}^u	0	$a^2\zeta$
0	$a^2\lambda\zeta$	$-a^2\lambda\zeta$	0	0	$E_{13}^u + a^2\zeta$	0
$a^3\lambda\zeta$	0	0	$-a^3\lambda\zeta$	$a^2\zeta$	0	E_{14}^u

Landau-Zener-Stückelberg (LZS) model using the properties of the potential curves in the vicinity of the avoided crossing. In terms of the diabatic $^5\Delta_g$ (labeled 1) and $^3\Sigma_g^-$ (labeled 2) potential curves, the probability of hopping is given by

$$P_{\text{hop}} = e^{-2\gamma}, \tag{26}$$

where

$$\gamma = \frac{\pi (V_{12}^d)^2}{v \left| \dfrac{d}{dR}(V_{11}^d - V_{22}^d) \right|}. \tag{27}$$

At the crossing distance, $R_x^d = 3.12$ Å, the slopes are $dV_{11}^d/dR = -0.0130$ a.u. and $dV_{22}^d/dR = 0.0268$ a.u., and the coupling is given by half the adiabatic splitting, i.e., $V_{12}^d = \frac{1}{2}(E_{22}^a - E_{11}^a) = 0.001\,63$ a.u. The crossing potential energy is $V_{11}^d = V_{22}^d = -0.0130$ a.u., which yields the velocity $v = (-2V_1/\mu)^{1/2} \approx 3.8 \times 10^{-4}$ a.u. for thermal collisions ($E \ll V_1$), neglecting the centrifugal potential (only small impact parameters can reach the crossing with the ion curve, which occurs very slightly below the asymptotic energy). Thus we obtain $\gamma = 0.55$ and $P_{\text{hop}} = 0.33$, sensibly independent of collision energy at low-to-moderate temperatures.

The cross section can then be written

$$\sigma = \pi b_{xd}^2 P_{\text{hop}} P_{\text{ion}}, \tag{28}$$

where b_{xd} is the largest impact parameter that will penetrate to the distance where the *upper* curve crosses the Hg_2^+ curve and P_{ion} is the conditional probability that ionization will then occur. A barrier in the *ab initio* incident curve at ~ 7 Å would preclude the reaction at $E = 0.000\,95$ a.u. With the barrier suppressed, the *upper limit* on the associative ionization cross section for $\text{Hg}(^3P_0) + \text{Hg}(^3P_0)$, obtained with $P_{\text{ion}} = 1$, would be $\sigma^{(nb)} = 67.9$ Å^2. The hotter atoms, contributing to the thermal average at 300 K, enable some reaction cross section even with the barrier, $\bar{\sigma}^{(b)} = 12.4$ Å^2, and, neglecting the barrier, $\bar{\sigma}^{(nb)} = 62.1$ Å^2. In this case, however, the black-sphere model is not expected to be realistic. The value of P_{ion} can be expected to be significantly smaller both

TABLE XIII. Spin-orbit matrix for 3_u states. $a \equiv 2^{-1/2}$.

$E_6^u + a^2\zeta$	$a^2\zeta$	$a^2\lambda\zeta$
$a^2\zeta$	$E_8^u + a^2\zeta$	$-a^2\lambda\zeta$
$a^2\lambda\zeta$	$-a^2\lambda\zeta$	$E_{14}^u + a^2\zeta$

TABLE XI. Spin-orbit matrix for 1_u states. $a \equiv 2^{-1/2}$, $b \equiv 3^{-1/2}$.

TABLE XIV. Distances R, potential energies V, and corresponding impact parameters b of black sphere (subscript s), crossing with molecular-ion curve if any (subscript x), and potential (including centrifugal) barrier outside R_s if any (subscript b), for potential curves contributing to chemi-ionization cross sections at collision energy 0.000 95 a.u. Numbers in square brackets denote powers of 10.

Reaction	Symmetry	Black sphere			Continuum crossing			Centrifugal barrier		
		R_s	V_s	b_s	R_x	V_x	b_x	R_b	V_b	b_b
$^3P_0+^3P_0$ [a]										
	0_g^+	4.00	-9.54[-3]	13.29	2.97	-6.20[-3]	8.15	7.60	1.19[-3]	0.00
$^3P_1+^3P_0$										
	0_g^-	4.00	-1.69[-2]	17.33	2.96	-1.39[-2]	11.70	7.71	9.74[-4]	0.00
	1_g	4.00	-8.31[-3]	12.49	3.20	-1.16[-2]	11.65	7.50	1.31[-3]	0.00
	0_u^-	4.00	-1.95[-4]	4.39	3.70	-7.12[-4]	4.89	7.59	7.12[-4]	3.80
$^3P_1+^3P_1$										
	0_g^+	4.00	-8.20[-3]	12.41	2.97	-2.23[-2]	14.69	7.68	2.82[-4]	6.44
	1_g	4.00	2.69[-4]	3.39	4.12	2.03[-4]	3.65	7.57	8.57[-4]	2.37
	2_g	4.00	-6.37[-3]	11.10	3.64	-1.03[-2]	12.54	7.54	1.51[-3]	0.00
$^3P_2+^3P_0$										
	2_g	4.00	-1.78[-3]	6.78	5.07	1.01[-4]	4.79	7.55	1.15[-3]	0.00
	2_u	4.00	-4.75[-3]	9.79	5.05	-3.98[-5]	5.15	7.59	1.01[-3]	0.00
$^3P_2+^3P_1$										
	1_g	4.00	8.97[-4]	0.95	8.13	2.08[-4]	7.19			
	3_g	4.00	-1.48[-2]	16.29	8.42	6.17[-4]	4.99	7.64	9.49[-4]	0.22
	1_u	4.00	-1.29[-3]	6.14	8.11	1.83[-4]	7.29	6.56	5.28[-4]	4.37
	2_u	4.00	-3.55[-3]	8.70	8.29	4.41[-4]	6.07	7.35	6.52[-4]	4.12
$^3P_2+^3P_2$										
	0_g^+	4.00	-1.34[-3]	6.22				4.68	5.97[-5]	4.53
	3_g	4.00	-4.78[-4]	4.90				7.63	9.83[-4]	0.00
	4_g	4.00	-2.22[-2]	19.76				7.73	6.36[-4]	4.44
	0_u^-	4.00	-5.67[-4]	5.05				4.94	4.74[-4]	3.50
$^1P_1+^3P_0$										
	0_g^-	4.00	-1.74[-2]	17.56				8.48	-4.5[-4]	10.30
	1_g	4.00	-3.19[-4]	4.62						
	0_u^-	4.00	-7.59[-4]	5.37						
	1_u	4.00	-8.00[-4]	5.43				4.11	-4.92[-4]	5.06
$^1P_1+^3P_1$										
	0_g^+	4.00	-1.41[-2]	15.92				9.47	-4.76[-4]	11.60
	0_g^+	4.00	-5.22[-3]	10.19				7.55	-3.29[-4]	8.76
	0_g^-	4.00	-1.74[-3]	6.73						
	1_g	4.00	-4.54[-3]	9.61				8.05	-3.35[-4]	9.36
	2_g	4.00	-2.28[-3]	7.37				4.17	-1.70[-3]	6.97
	0_u^+	4.00	-2.19[-2]	19.62				9.52	-4.76[-4]	11.66
	0_u^+	4.00	-2.09[-2]	19.20				5.99	-1.05[-3]	8.70
	1_u	4.00	-7.64[-3]	12.02				7.99	-3.98[-4]	9.52
	1_u	4.00	-5.13[-3]	10.12				7.36	-2.01[-4]	8.10
$^1P_1+^3P_2$										
	0_g^+	4.00	-1.18[-2]	14.67				7.53	-3.79[-4]	8.91
	1_g	4.00	-1.43[-2]	16.00				7.56	-4.45[-4]	9.16
	1_g	4.00	6.02[-5]	3.87						
	2_g	4.00	-2.14[-2]	19.39				9.47	-4.76[-4]	11.60
	1_u	4.00	-2.54[-2]	21.05				7.77	-4.16[-4]	9.32
	1_u	4.00	8.23[-4]	1.46						
	2_u	4.00	-2.11[-2]	19.26				9.46	-4.77[-4]	11.59
	3_u	4.00	-6.08[-3]	10.88				5.89	9.52[-5]	5.59
$^1P_1+^1P_1$										
	0_g^+	4.00	-2.57[-2]	21.18				10.00	-5.29[-4]	12.48
	0_g^+	4.00	-5.80[-3]	10.66				7.39	-7.30[-4]	9.83
	1_g	4.00	-3.84[-3]	8.98				10.00	1.55[-3]	0.00
	2_g	4.00	-8.20[-3]	12.41				6.85	4.81[-4]	4.81
	0_u^-	4.00	-1.57[-2]	16.76				6.96	-4.74[-4]	8.52

[a]With curve crossing.
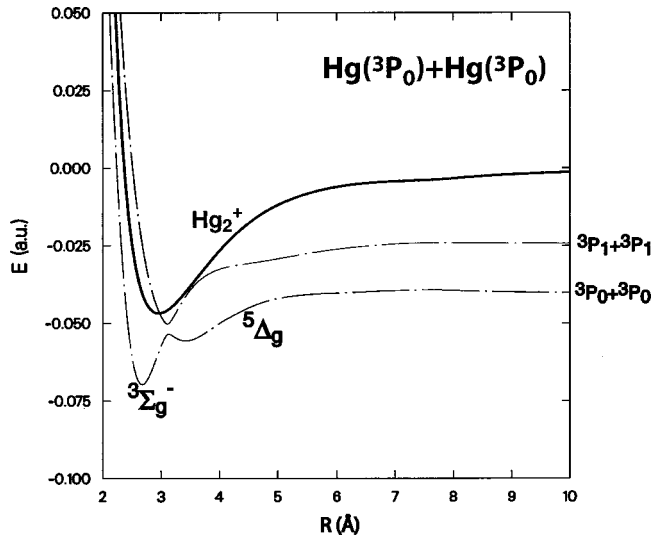
FIG. 3. Potential-energy curves contributing to chemi-ionization in Hg($^3P_0$)+Hg($^3P_0$) collisions. In this and subsequent figures, the molecular symmetry [in Hund's case (c)] is designated as follows: number dots = 1 + angular momentum of g states, number dashes = 1 + angular momentum of u states, except 0_g^- = dot dash, and 0_u^+ = dash dot.

because the time spent in the continuum is very short and the state that penetrates the continuum is primarily a quintet spin state, which has zero width. In any event, the upper limit obtained is already smaller than the value 160 ± 40 Å^2 given experimentally by Sepman *et al.* [11], which has been challenged experimentally by Majetich *et al.* [12,9]. Experimental evidence against chemi-ionization in $^3P_0+^3P_0$ collisions was also presented by Sibata *et al.* [34].

2. Hg($^3P_1$)+Hg($^3P_0$)

In the case of Hg($^3P_1$)+Hg($^3P_0$), there are four potential curves that arise from the asymptote, as shown in Fig. 4. The asymptote is lower than the Hg$^+$+Hg asymptote but all the curves cross the Hg$_2^+$ curve at smaller distances and, in principle, can contribute to associative ionization with their respective statistical weights. One of them (1_u) is significantly repulsive at its crossing with the molecular ion ($V = 0.0043$ a.u.) and can be practically ignored for thermal collisions. The 1_g curve barely penetrates the continuum before it is repelled by an avoided crossing with a curve of the same symmetry coming from the $^3P_1+^3P_1$ asymptote. This crossing is more weakly avoided than the one discussed in Sec. III B 1, and a similar LZS analysis yields a hopping probability of 0.78. That is, most of the 1_g flux will continue further into the continuum and, in keeping with the upper-bound nature of the present estimates, we will ignore the possible reduction. The cross-section contributions, calculated with ($\sigma^{(b)}$) and without ($\sigma^{(nb)}$) the long-range barriers,
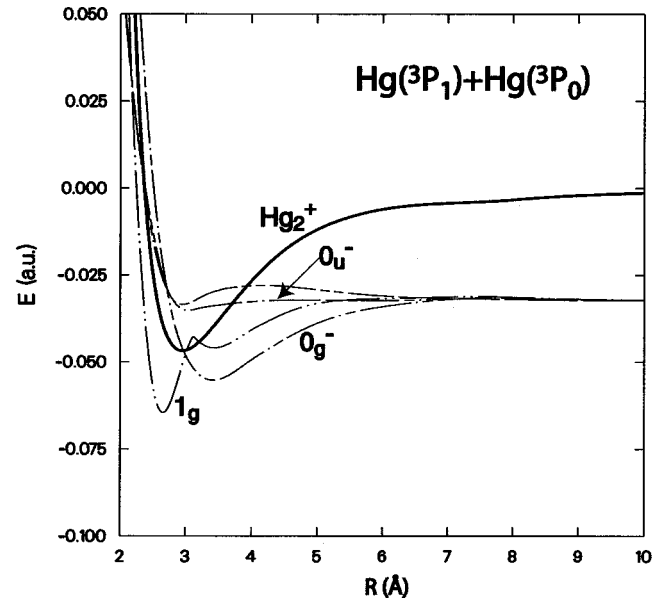
FIG. 4. Potential-energy curves contributing to chemi-ionization in Hg($^3P_1$)+Hg($^3P_0$) collisions. See Fig. 3 caption for designation of symmetries; the most important curves are also labeled.

at energy $E=kT$ and thermal average ($\bar{\sigma}^{(b)}$ and $\bar{\sigma}^{(nb)}$) at $T = 300$ K, are[4]

State	$\sigma^{(b)}$	$\sigma^{(nb)}$	$\bar{\sigma}^{(b)}$	$\bar{\sigma}^{(nb)}$
0_g^-	0.00	430.20	62.75	430.20
1_g	0.00	136.40	36.55	136.36
0_u^-	45.35	46.51	41.47	46.11
1_u	0.00	0.00	0.53	0.53
Total	7.56	124.92	29.73	125.02

$$(29)$$

With barriers, the Maxwellian tail is needed to get contributions from the 0_g^- and 1_g states and substantially increases the cross section (by a factor of ~4). In the absence of barriers, the thermal spread of energies has little effect.

This cross section has been the subject of experiments that utilize collisions with N$_2$ to convert Hg($^3P_1$) to Hg($^3P_0$) [34]. Our value may be compared with the experimental values 460 Å^2 (no error bar given) of Tan and von Engel [10] and 99 ± 25 Å^2 of Majetich *et al.* [9].[5] This

---

[4]Cross sections are given in units of Å^2 ($=10^{-16}$ cm^2). The *accuracy* of the cross sections is not expected to be better than $\sim10\%$, though the *precision* is to the figures given.

[5]The value of 139 ± 34 Å^2 given in Ref. [9] apparently resulted from use of the atomic mass instead of the reduced mass in converting the measured rate constant (there is also a typo in the rate constant given in this paper; it should be 2.54×10^{-10} cm^3 s^{-1} instead of 2.54×10^{-8} cm^3 s^{-1}). Another simulation of this experiment yielded $k_{AI}=1.65\times10^{-10}$ cm^3 s^{-1}, which corresponds to $\sigma_{AI}=64$ Å^2 [9].
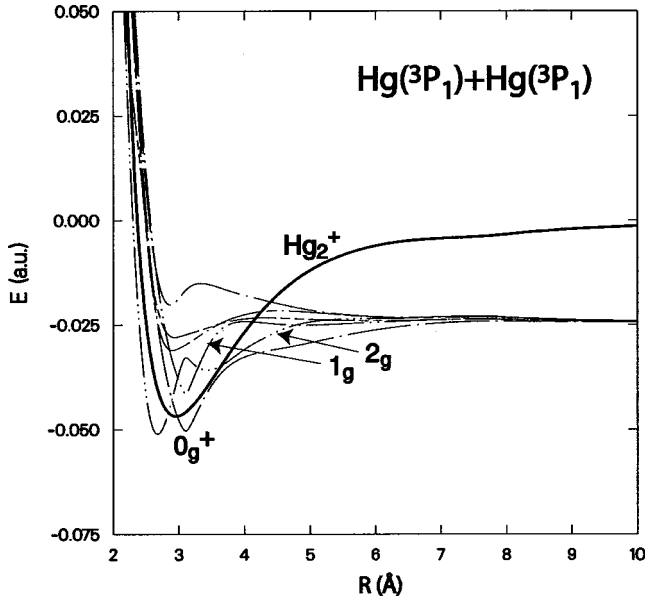
FIG. 5. Potential-energy curves contributing to chemi-ionization in $Hg(^3P_1) + Hg(^3P_1)$ collisions. See Fig. 3 caption for designation of symmetries.
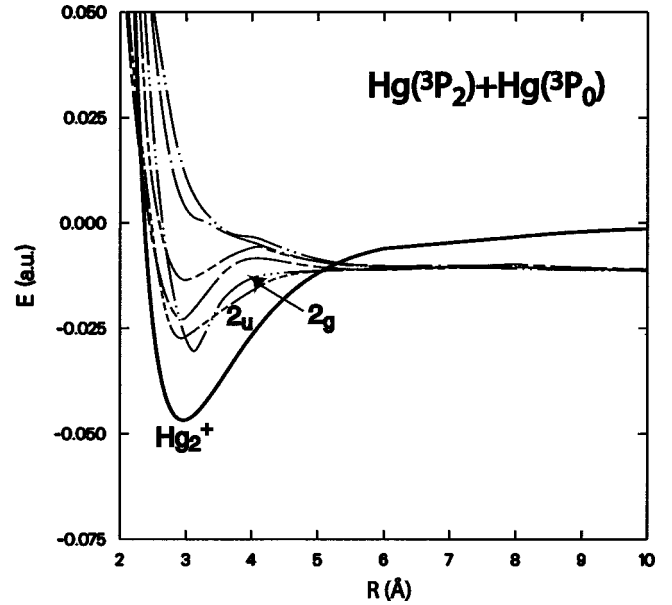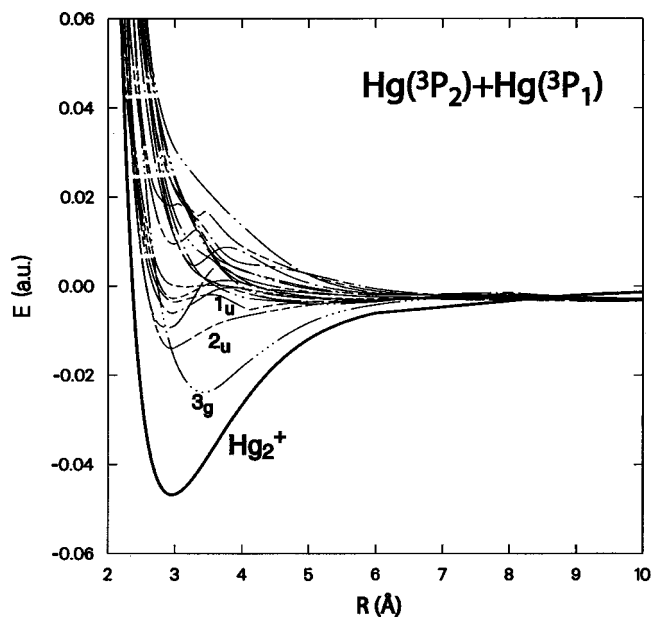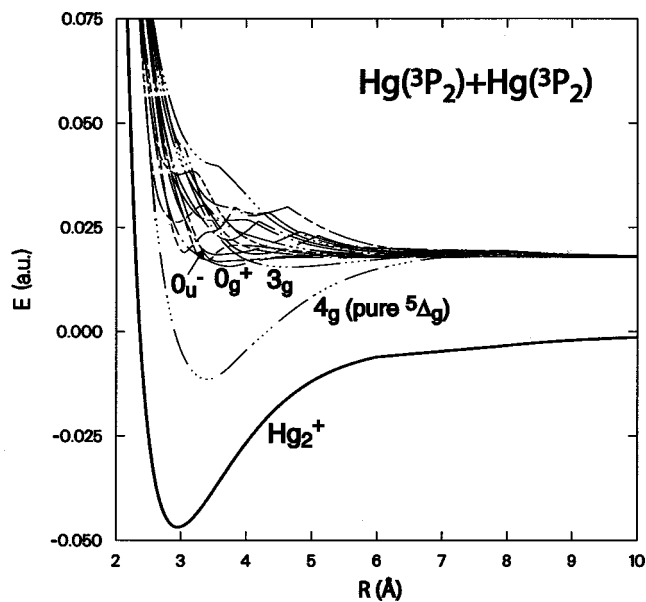

FIG. 6. Potential-energy curves contributing to chemi-ionization in $Hg(^3P_2) + Hg(^3P_0)$ collisions. See Fig. 3 caption for designation of symmetries.

agreement suggests that the black-sphere model yields reasonable estimates for cases where the continuum is amply accessed.

3. $Hg(^3P_1) + Hg(^3P_1)$

Of the six potential curves arising from $Hg(^3P_1) + Hg(^3P_1)$, shown in Fig. 5, half, representing 5/9 of the total flux, are attractive and contribute to associative ionization in thermal-energy collisions. Here, and in the potential curves from higher asymptotes, there are numerous curve crossings, generally weakly avoided, that complicate the interactions but have no effect on the ionization cross sections within the black-sphere model. The 1_g curve is attractive but rather flat outside the crossing into the continuum, so admits only small-impact-parameter reactions. The largest contribution comes from the strongly attractive curve of 0_g^+ symmetry. The cross-section contributions are

State	$\sigma^{(b)}$	$\sigma^{(nb)}$	$\bar{\sigma}^{(b)}$	$\bar{\sigma}^{(nb)}$
0_g^+	130.33	477.78	132.38	468.69
0_g^+	0.00	0.00	0.06	0.06
1_g	17.71	36.04	34.51	38.12
2_g	0.00	67.63	30.01	68.41
0_u^-	0.00	0.00	3.42	3.42
1_u	0.00	0.00	16.29	16.29
Total	18.42	76.12	33.06	79.76

$$(30)$$

Thus it would appear that associative ionization in $Hg(^3P_1)$ self-collisions could be competitive with associative ionization in collisions of $Hg(^3P_1)$ with $Hg(^3P_0)$ if the populations are comparable. As in the case of $Hg(^3P_1)$

$+ Hg(^3P_0)$, the cross section is significantly reduced by the potential barriers. The temperature dependence is not as strong even with the barriers.

4. $Hg(^3P_2) + Hg(^3P_0)$

Collisions between metastable atoms may be most important in the afterglow after the allowed $Hg(^3P_1)$ and $Hg(^1P_1)$ populations have radiatively decayed [40,2,41]. Only the 2_g and 2_u potential curves from $Hg(^3P_2) + Hg(^3P_0)$, shown in Fig. 6, are attractive (apart from weak barriers at ~ 7 Å). Two other curves, 0_u^+ and 1_u, become attractive at small R due to curve crossings, but are too repulsive outside the continuum crossing to accommodate chemi-ionization. The cross-section contributions are

State	$\sigma^{(b)}$	$\sigma^{(nb)}$	$\bar{\sigma}^{(b)}$	$\bar{\sigma}^{(nb)}$
0_g^+	0.00	0.00	0.04	0.04
1_g	0.00	0.00	0.01	0.01
2_g	0.00	72.20	35.80	69.99
0_u^+	0.00	0.00	2.39	2.39
1_u	0.00	0.00	0.12	0.12
2_u	0.00	83.47	46.59	83.11
Total	0.00	31.13	16.75	30.89

$$(31)$$

This cross section is relatively small but possibly still significant since both states are metastable.

5. $Hg(^3P_2) + Hg(^3P_1)$

The cross section for $Hg(^3P_2) + Hg(^3P_1)$ is potentially important in discharges for the same reason as $Hg(^3P_1)$

FIG. 7. Potential-energy curves contributing to chemi-ionization in $Hg(^3P_2)+Hg(^3P_1)$ collisions. See Fig. 3 caption for designation of symmetries.
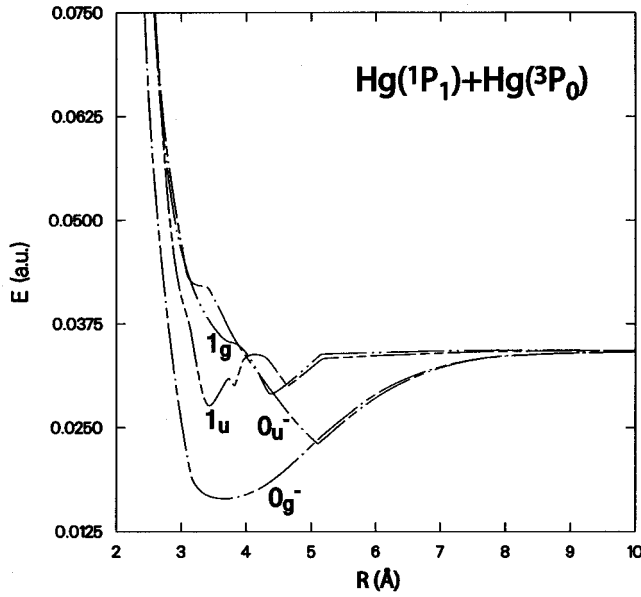

FIG. 8. Potential-energy curves contributing to chemi-ionization in $Hg(^3P_2)+Hg(^3P_2)$ collisions. See Fig. 3 caption for designation of symmetries.

$+Hg(^3P_0)$, but has not been measured. Theoretically, the radiative allowed/metastable nature of the states is of little relevance to the chemi-ionization cross sections. As listed in Table II, a large number (18) of distinct potential curves come from the $^3P_2+^3P_1$ interaction. As shown in Fig. 7, the asymptotic energy is just below that of the molecular ion, and all these potential curves cross into the ionization continuum at large distances (~ 8 Å). However, only four $(1_g,3_g,1_u,2_u)$ are sufficiently attractive that associative ionization is likely in a thermal-energy collision. The cross-section contributions are

State	$\sigma^{(b)}$	$\sigma^{(nb)}$	$\bar{\sigma}^{(b)}$	$\bar{\sigma}^{(nb)}$
0_g^+	0.00	0.00	0.00	0.00
0_g^-	0.00	0.00	5.68	5.68
0_g^-	0.00	0.00	0.04	0.04
1_g	2.83	2.83	19.92	19.92
1_g	0.00	0.00	0.70	0.70
1_g	0.00	0.00	0.00	0.00
2_g	0.00	0.00	1.73	1.73
2_g	0.00	0.00	0.03	0.03
3_g	0.16	78.09	64.84	114.34
0_u^+	0.00	0.00	0.32	0.32
0_u^-	0.00	0.00	2.98	2.98
0_u^-	0.00	0.00	0.01	0.01
1_u	60.05	99.22	60.15	87.57
1_u	0.00	0.00	0.15	0.15
1_u	0.00	0.00	0.00	0.00
2_u	53.30	115.78	73.11	96.82
2_u	0.00	0.00	0.70	0.70

State	$\sigma^{(b)}$	$\sigma^{(nb)}$	$\bar{\sigma}^{(b)}$	$\bar{\sigma}^{(nb)}$
3_u	0.00	0.00	2.75	2.75
Total	7.76	19.73	15.24	21.95

$$(32)$$

This is considerably smaller than the $Hg(^3P_1)$ $+Hg(^3P_0)$ cross section. Under somewhat hot thermal conditions, Penning ionization may also occur but is relatively unlikely because the expected Franck-Condon behavior of the transition will usually result in a molecular ion deep in its potential well.

6. $Hg(^3P_2)+Hg(^3P_2)$

Because of its high statistical weight and metastability, self collisions of $Hg(^3P_2)$ may be the most common collisions under some discharge conditions at late times. Thus this cross section is of particular concern. Of the 15 associated potential curves, shown in Fig. 8, only the 4_g state is strongly attractive. In fact, this potential curve suffers no avoided crossings and is the most attractive of all the potential curves resulting from the $Hg(6s6p)+Hg(6s6p)$ interactions. If chemi-ionization could occur in this state, the black-sphere approximation would give $\sim 1 \times 10^{-14}$ cm^2. However, the 4_g state is pure $^5\Delta_g$, unmixed by spin-orbit coupling, and quintet states are not coupled to the continuum. Consequently there are only small contributions in self collisions of $Hg(^3P_2)$, mainly by three other states,

| State	$\sigma^{(b)}$	$\sigma^{(nb)}$	$\bar{\sigma}^{(b)}$	$\bar{\sigma}^{(nb)}$
0_g^+	64.48	64.48	62.37	62.37
0_g^+	0.00	0.00	0.21	0.21
0_g^+	0.00	0.00	0.01	0.01

FIG. 9. Potential-energy curves contributing to chemi-ionization in $Hg(^1P_1)+Hg(^3P_0)$ collisions. See Fig. 3 caption for designation of symmetries.

State	$\sigma^{(b)}$	$\sigma^{(nb)}$	$\bar{\sigma}^{(b)}$	$\bar{\sigma}^{(nb)}$
1_g	0.00	0.00	0.00	0.00
1_g	0.00	0.00	0.00	0.00
2_g	0.00	0.00	0.13	0.13
2_g	0.00	0.00	0.00	0.00
3_g	0.00	75.56	37.81	75.56
4_g	62.00	858.45	94.56	858.45
0_u^-	38.41	38.41	42.61	42.61
0_u^-	0.00	0.00	0.25	0.73
1_u	0.00	0.00	2.48	2.48
1_u	0.00	0.00	0.00	0.00
2_u	0.00	0.00	3.34	3.34
3_u	0.00	0.00	0.39	0.39
Total	4.12	10.16	7.75	10.79

$$(33)$$

Thus, chemi-ionization destruction of the $^3P_2$ state, even when combined with the contributions of collisions with the $^3P_0$ and $^3P_1$ states, is predicted to be relatively small. The cross section is small even with the barriers suppressed; likewise the hot thermal tail does not greatly enhance it. In spite of the asymptote being well above that of the ion, the Franck-Condon principle suggests that the ionization that does occur will be mainly associative since the upper-level wells are shallow.

7. $Hg(^1P_1)+Hg(^3P_0)$

The $Hg(^1P_1)$ state rapidly radiates, $A=7.46\times10^8$ s^{-1} [42], and so chemi-ionization might not be expected to be competitive. However, this radiation is often strongly trapped under gaseous discharge conditions, so it is not a foregone conclusion that this is true. First we consider its collisions
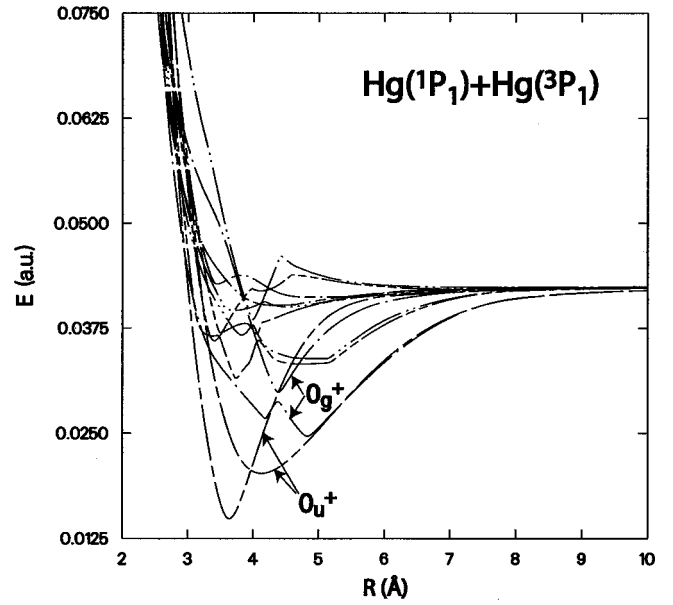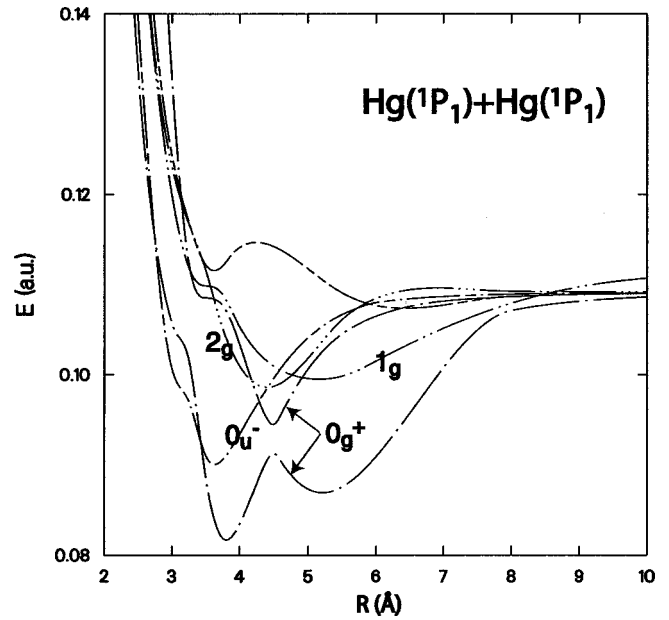

FIG. 10. Potential-energy curves contributing to chemi-ionization in $Hg(^1P_1)+Hg(^3P_1)$ collisions. See Fig. 3 caption for designation of symmetries.

with the metastable $Hg(^3P_0)$. In this case, all four of the potential curves, shown in Fig. 9, are attractive and can contribute at thermal energies, though the reaction is dominated by the strongly attractive 0_g^- state. The cross-section contributions are

State	$\sigma^{(b)}$	$\sigma^{(nb)}$	$\bar{\sigma}^{(b)}$	$\bar{\sigma}^{(nb)}$
0_g^-	333.37	968.36	309.83	968.35
1_g	67.12	67.12	65.98	67.12
0_u^-	90.44	90.44	90.44	90.44
1_u	80.58	80.58	80.41	80.41
Total	119.87	225.70	115.51	225.64

$$(34)$$

For the $Hg(^1P_1)$ reactions the energies of the ejected electrons will be relatively higher ($\gtrsim1$ eV) than for the triplet-triplet reactions, and, by point 4 in Sec. III A, the width may be smaller and the black-sphere model more of an overestimate of the cross section. Even so, for the reaction rate to be competitive with the vacuum radiative loss rate, a $Hg(^3P_0)$ number density of $\sim10^{18}$ cm^{-3} would be required, which would be quite high. However, with very strong radiation trapping, the collisional rate could still be significant.

8. $Hg(^1P_1)+Hg(^3P_1)$

Collisions between *two* allowed states are even less likely. The vacuum radiative decay rate of $Hg(^3P_1)$ is $A=8.40\times10^6$ s^{-1} [42]. However, most of the $Hg(^1P_1)+Hg(^3P_1)$ potential curves, shown in Fig. 10, are attractive,
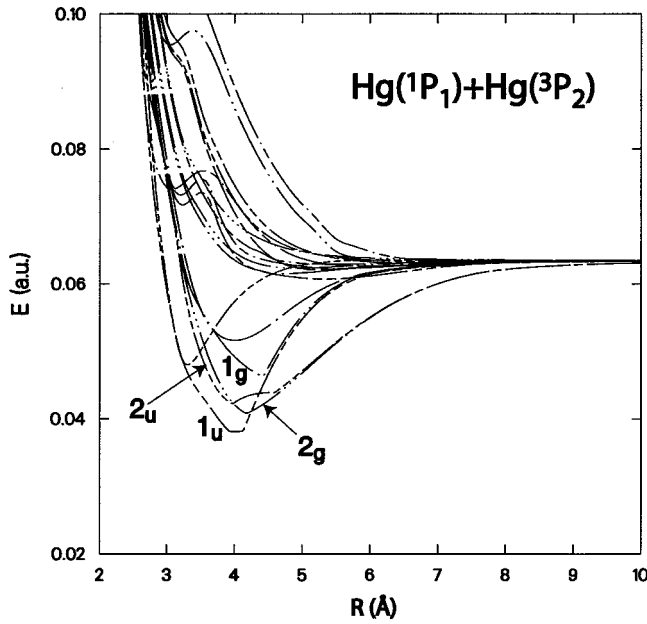
FIG. 11. Potential-energy curves contributing to chemi-ionization in $Hg(^1P_1) + Hg(^3P_2)$ collisions. See Fig. 3 caption for designation of symmetries.

especially the two 0_u^+ states, and the black-sphere model yields a quite large cross section, with contributions

State	$\sigma^{(b)}$	$\sigma^{(nb)}$	$\bar{\sigma}^{(b)}$	$\bar{\sigma}^{(nb)}$
0_g^+	422.92	796.45	389.69	796.45
0_g^+	241.11	326.36	207.10	326.36
0_g^-	142.48	142.48	126.16	142.48
1_g	275.35	290.29	211.89	290.29
1_g	0.00	0.00	1.07	1.07
2_g	152.65	152.65	121.98	152.62
0_u^+	427.41	1209.07	401.14	1209.07
0_u^+	237.72	446.76	210.69	446.76
0_u^-	0.00	0.00	17.02	17.02
1_u	284.60	396.65	245.52	396.65
1_u	206.23	240.17	175.34	238.87
2_u	0.00	0.00	14.03	14.03
Total	183.85	282.26	160.64	284.73

$$(35)$$

The curves with symmetry pairs, 0_g^+, 1_g, 0_u^+, and 1_u, exhibit weakly avoided crossings at $R \approx 4$ Å. The second 1_g curve has energy at $R = 4$ Å below the asymptote, but has a large barrier outside due to a higher curve crossing. The Penning component of the total chemi-ionization reaction could be significant in $Hg(^1P_1) + Hg(^3P_1)$ collisions since some of the potential curves are more attractive than the Hg_2^+ curve near $R = 4$ Å.

9. $Hg(^1P_1) + Hg(^3P_2)$

The potential curves for $Hg(^1P_1) + Hg(^3P_2)$ are shown in Fig. 11. Half the flux enters in attractive potential curves and

FIG. 12. Potential-energy curves contributing to chemi-ionization in $Hg(^1P_1) + Hg(^1P_1)$ collisions. See Fig. 3 caption for designation of symmetries.

the black-sphere cross-section contributions are

State	$\sigma^{(b)}$	$\sigma^{(nb)}$	$\bar{\sigma}^{(b)}$	$\bar{\sigma}^{(nb)}$
0_g^+	249.28	573.16	229.28	572.85
0_g^-	0.00	0.00	1.02	1.02
0_g^-	0.00	0.00	0.00	0.00
1_g	263.64	753.94	240.52	752.12
1_g	47.08	47.08	47.08	47.08
1_g	0.00	0.00	0.00	0.00
2_g	422.85	1180.83	396.15	1180.83
2_g	0.00	0.00	13.38	13.38
3_g	0.00	0.00	0.12	0.12
0_u^+	0.00	0.00	0.02	0.02
0_u^-	0.00	0.00	3.21	3.21
0_u^-	0.00	0.00	0.01	0.01
1_u	272.62	796.21	253.05	796.21
1_u	6.71	6.71	21.62	21.62
1_u	0.00	0.00	0.00	0.00
2_u	422.21	1164.83	395.44	1164.83
2_u	0.00	0.00	0.01	0.01
3_u	98.07	132.57	93.25	132.51
Total	110.52	291.25	105.16	293.15

$$(36)$$

This reaction is likely to have the largest Penning ionization fraction.

10. $Hg(^1P_1) + Hg(^1P_1)$

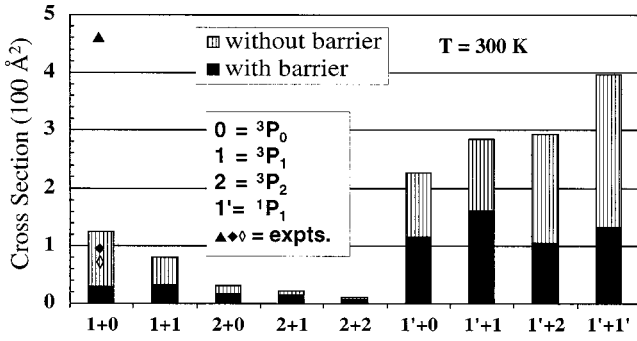For completeness, we also treat $Hg(^1P_1) + Hg(^1P_1)$, shown in Fig. 12. Even though the black-sphere cross section, with contributions

FIG. 13. Thermally averaged cross sections at 300 K for the $Hg(6s6p)+Hg(6s6p)$ chemi-ionization reactions in the black-sphere model [see Sec. III B 1 for discussion of the $Hg(^3P_0)$ $+Hg(^3P_0)$ cross section, not shown]. The lower values designate the calculation with the unadjusted *ab initio* potential curves, the higher values the cross section with long-range barriers suppressed. The experimental values for $Hg(^3P_1)+Hg(^3P_0)$ are from Tan and von Engel (solid triangle) [10], Majetich *et al.* (solid diamond) [9], and an alternative analysis of Majetich (open diamond) [9].

State	$\sigma^{(b)}$	$\sigma^{(nb)}$	$\bar{\sigma}^{(b)}$	$\bar{\sigma}^{(nb)}$
0_g^+	488.99	1245.02	472.20	1244.99
0_g^+	303.36	356.93	249.84	356.93
1_g	0.00	253.20	45.62	253.20
2_g	72.75	483.91	84.56	483.91
0_u^-	228.13	495.66	206.30	495.66
1_u	0.00	0.00	0.15	0.15
Total	129.55	396.87	132.11	396.90

$$(37)$$

are largest of all, it is not expected that this reaction, involving two radiatively short-lived reactants, will be significant under usual discharge conditions.

IV. CONCLUSIONS

The present calculations suggest that the experimental disagreement, as to whether $Hg(^3P_0)$ associative ionization is mainly due to self collisions or collisions with $Hg(^3P_1)$, is resolved in favor of $Hg(^3P_1)$. The $Hg(^3P_0)+Hg(^3P_0)$ cross section would appear to to quite small, even though an avoided curve crossing could still make it non-negligible. All pairs of $Hg(6s6p)$ atoms, except possibly for $Hg(^3P_0)$ $+Hg(^3P_0)$, will have significant chemi-ionization cross sections, but the cross sections for $^3P_2$ with itself and with the other triplet states are predicted to be relatively small. Chemi-ionization cross sections for the metastable-metastable collisions are found to be considerably smaller than for the allowed atomic states, $Hg(^3P_1)$ and especially $Hg(^1P_1)$. There is little *a priori* reason to expect such a relation, but it is serendipitous for lamp efficiency. Associative ionization is expected to dominate in all cases though
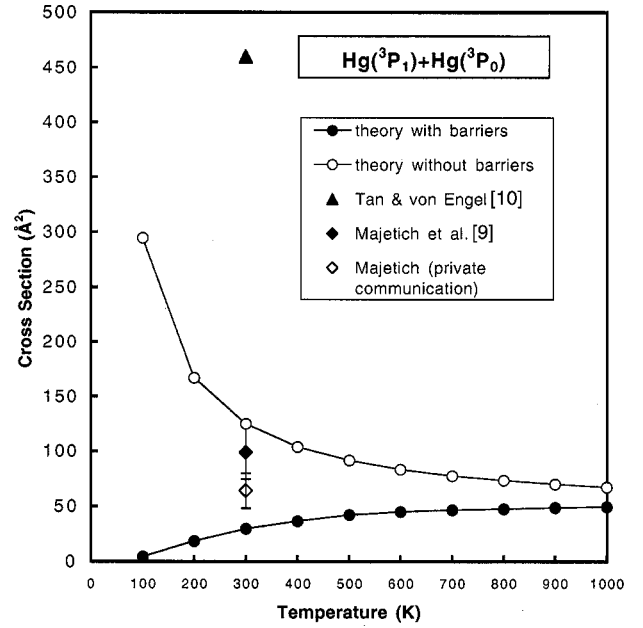

FIG. 14. Thermally averaged cross sections for chemi-ionization in $Hg(^3P_1)+Hg(^3P_0)$ collisions as a function of temperature: calculated with long-range potential barriers (open circles) and without long-range potential barriers (solid circles), and experiments at T ≈ 300 K of Tan and von Engel (solid triangle) [10], Majetich *et al.* (solid diamond) [9], and alternative analysis of Majetich (open diamond) [9].
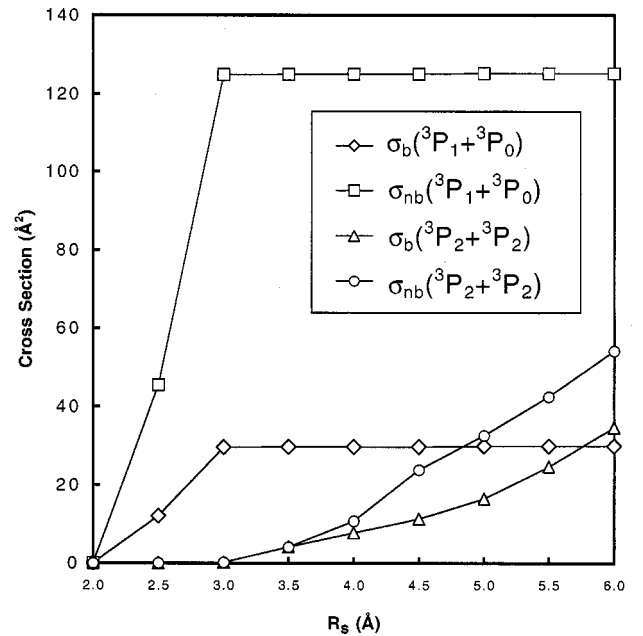

FIG. 15. Dependence of the chemi-ionization cross sections at 300 K for $Hg(^3P_1)+Hg(^3P_0)$ and $Hg(^3P_2)+Hg(^3P_2)$ on the black-sphere radius R_s, with and without potential barriers. The cross section for the former reaction, in which only associative ionization can occur, is limited by the crossing distance between the neutral and molecular-ion potential curves. The cross section for the latter, in which ionization is *energetically* allowed even at infinity, would increase quadratically with very large (*unphysical*) R_s.

the Hg($^1P_1$) reactions may have non-negligible Penning ionization cross sections.

Several of the *ab initio* potential curves exhibit small barriers, which, if correct, could dramatically reduce the chemi-ionization cross sections at temperatures below ~ 300 K. The thermal average cross sections at 300 K are shown in Fig. 13, with and without the effect of these barriers. The cross sections for different pairs of reactant atomic states are quite different, and an accurate predictive model of mercury lamps would need to account for the separate populations. The barriers and temperature dependences are most manifest when both of the interacting atoms are in triplet states. In all these cases, the cross sections increase as a function of energy and temperature in the range 0–1000 K. On the other hand, when one of the atoms is $^1P_1$, the cross sections are decreasing functions. If the barriers are suppressed, all the cross sections tend to be flat or decrease with increasing energy and temperature.

An example is shown in Fig. 14 for the Hg($^3P_1$) $+$ Hg($^3P_0$) reaction, which seems to be most amenable to afterglow experiments. The more recent experimental measurements, at ~ 300 K, fall in between the results obtained with and without the potential barriers in question and do not provide much basis for discrimination. However, a future measurement of the temperature dependence, over a range ~ 200–400 K, could clearly establish the reality of the barriers. The measurement of the energy dependence in a cross-beam experiment, even without absolute calibration, would also be informative.

The present calculations were done in the black-sphere model. The choice of the black-sphere distance R_s is based on the overlap of the atomic orbitals but is still somewhat arbitrary. In addition, the assumption that ionization is complete within R_s is unverified, though it is a reasonable expectation for low-energy collisions. The chemi-ionization cross sections with reactants for which only associative ionization is energetically possible, as shown in Fig. 15 for Hg($^3P_1$) $+$ Hg($^3P_0$), depend rather weakly on reasonable values of R_s. For reactants with energies above the atomic ionization threshold, as is the case for the Hg($^3P_2$) $+$ Hg($^3P_2$) reaction shown in Fig. 15, the sensitivity to R_s is considerably greater, even within the range $3.5 < R_s < 4.0$ which might be considered the uncertainty. Comparison with the experimental Hg($^3P_1$) $+$ Hg($^3P_0$) cross sections suggests that the black-sphere model is realistic. Of course, no value of R_s can yield the actual energy-dependent results and, in future work, we plan to calculate the autoionization widths and eliminate this approximation.

[1] J. Weiner, F. Masnou-Seeuws, and A. Giusti-Suzor, Adv. At., Mol., Opt. Phys. **26**, 209 (1989).

[2] L. Vriens, R. A. J. Keijser, and F. A. S. Ligthard, J. Appl. Phys. **49**, 3807 (1978).

[3] Y. Sakai, S. Sawada, and H. Tagashira, J. Phys. D **22**, 276 (1989).

[4] S. Sawada, Y. Sakai, and H. Tagashira, J. Phys. D **22**, 282 (1989).

[5] J. Maya and R. Lagushenko, Adv. At., Mol., Opt. Phys. **26**, 321 (1989).

[6] M. Yousfi, G. Zissis, A. Alkaa, and J. J. Damelincourt, Phys. Rev. A **42**, 978 (1990).

[7] G. Zissis, P. Bénétruy, and I. Bernat, Phys. Rev. A **45**, 1135 (1992).

[8] G. G. Lister and S. E. Coe, Comput. Phys. Commun. **75**, 160 (1993).

[9] S. Majetich, C. A. Tomczyk, and J. R. Wiesenfeld, J. Appl. Phys. **69**, 563 (1991); S. Majetich (private communication).

[10] K. L. Tan and A. von Engel, J. Phys. D **1**, 258 (1968).

[11] V. Yu. Sepman, V. A. Sheverev, and V. Vuinovich, Opt. Spektrosk. **56**, 590 (1984) [Opt. Spectrosc. **56**, 361 (1984)].

[12] S. Majetich, E. M. Boczar, and J. R. Wiesenfeld, J. Appl. Phys. **66**, 475 (1989).

[13] S. Majetich, C. A. Tomczyk, and J. R. Wiesenfeld, Phys. Rev. A **41**, 6085 (1990).

[14] J. S. Cohen, R. L. Martin, and N. F. Lane, Phys. Rev. A **31**, 152 (1985).

[15] B. H. Lengsfield, R. L. Martin, P. W. Saxe, T. V. Russo, M. Page, B. I. Schneider, M. O. Braunstein, P. J. Hay, and A. K. Rappé, MESA (LANL, Los Alamos 1993).

[16] W. J. Stevens, H. Basch, and M. Krauss, J. Chem. Phys. **81**, 6026 (1984).

[17] W. J. Stevens, M. Krauss, H. Basch, and P. G. Jasien, Can. J. Chem. **70**, 612 (1992).

[18] P. J. Hay, T. H. Dunning, and R. C. Raffenetti, J. Chem. Phys. **65**, 2679 (1976).

[19] F. H. Mies, W. J. Stevens, and M. Krauss, J. Mol. Spectrosc. **72**, 303 (1978).

[20] K. C. Celestino and W. C. Ermler, J. Chem. Phys. **81**, 1872 (1984).

[21] K. Balasubramanian, K. K. Das, and D. W. Liao, Chem. Phys. Lett. **195**, 487 (1992).

[22] E. Czuchaj, F. Rebentrost, H. Stroll, and H. Preuss, Chem. Phys. **214**, 277 (1997).

[23] M. D. Morse, Chem. Rev. **86**, 1049 (1986).

[24] M. M. Gleichmann and B. A. Hess, Chem. Phys. Lett. **227**, 229 (1994).

[25] E. R. Davidson, J. Comput. Phys. **17**, 87 (1975).

[26] The numerical values of these potential curves are available at http://www.t4.lanl.gov

[27] J. K. Knipp, Phys. Rev. **53**, 734 (1938).

[28] F. L. Arnot and J. C. Milligan, Proc. R. Soc. London **153**, 359 (1936).

[29] A. B. Callear and K.-L. Lai, Chem. Phys. Lett. **75**, 234 (1980).

[30] S. Linn, C. L. Liao, C. X. Liao, J. J. M. Brom, and C. Y. Ng, Chem. Phys. Lett. **105**, 645 (1984).

[31] H. H. Michels, R. H. Hobbs, and J. W. D. Connolly, Chem. Phys. Lett. **68**, 549 (1979).

[32] V. E. Jog and M. A. Biondi, J. Phys. B **14**, 4719 (1981).

[33] P. J. Harbour, J. Phys. B **4**, 528 (1971).

[34] A. Sabata, M. Takahasi, H. Mikuni, H. Horiguchi, and S. Tsuchiya, Bull. Chem. Soc. Jpn. **52**, 15 (1979).

[35] B. Cabaud, A. Horeau, and P. Melinon, J. Phys. D **13**, 1831 (1980).

[36] A. D. Becke, J. Chem. Phys. **98**, 5648 (1993).

[37] M. J. Frisch *et al.*, GAUSSIAN 98, Revision A4 (Gaussian Inc., Pittsburgh, 1998).

[38] J. S. Cohen and B. Schneider, J. Chem. Phys. **61**, 3230 (1974).

[39] W. C. Martin, J. Sugar, and J. L. Tech, Phys. Rev. A **6**, 2022 (1972).

[40] O. Bochkova, S. Frish, and Yu. Tolmachev, Opt. Commun. **7**, 423 (1973).

[41] Y. Sukai, S. Sawada, and H. Tagashira, J. Phys. D **22**, 276 (1989).

[42] D. C. Morton, Astrophys. J., Suppl. Ser. **130**, 403 (2000).